CM^2 Magazine

第 137 期

南方科技大学海洋磁学中心主编

https://cm2.sustech.edu.cn/

创刊词

海洋是生命的摇篮，是文明的纽带。地球上最早的生命诞生于海洋，海洋里的生命最终进化成了人类，人类的文化融合又通过海洋得以实现。人因海而兴。

人类对海洋的探索从未停止。从远古时代美丽的神话传说，到麦哲伦的全球航行，再到现代对大洋的科学钻探计划，海洋逐渐从人类敬畏崇拜幻想的精神寄托演变成可以开发利用与科学研究的客观存在。其中，上个世纪与太空探索同步发展的大洋科学钻探计划将人类对海洋的认知推向了崭新的纬度：深海（deep sea）与深时（deep time）。大洋钻探计划让人类知道，奔流不息的大海之下，埋藏的却是亿万年的地球历史。它们记录了地球板块的运动，从而使板块构造学说得到证实；它们记录了地球环境的演变，从而让古海洋学方兴未艾。

在探索海洋的悠久历史中，从大航海时代的导航，到大洋钻探计划中不可或缺的磁性地层学，磁学发挥了不可替代的作用。这不是偶然，因为从微观到宏观，磁性是最基本的物理属性之一，可以说，万物皆有磁性。基于课题组的学科背景和对海洋的理解，我们对海洋的探索以磁学为主要手段，海洋磁学中心因此而生。

海洋磁学中心，简称 CM^2，一为其全名“Centre for Marine Magnetism”的缩写，另者恰与爱因斯坦著名的质能方程 $E = MC^2$ 对称，借以表达我们对科学巨匠的敬仰和对科学的不懈追求。

然而科学从来不是单打独斗的产物。我们以磁学为研究海洋的主攻利器，但绝不仅限于磁学。凡与磁学相关的领域均是我们关注的重点。为了跟踪反映国内外地球科学特别是与磁学有关的地球科学领域的最新研究进展，海洋磁学中心特地主办 CM^2 Magazine，以期与各位地球科学工作者相互交流学习、合作共进！

“海洋孕育了生命，联通了世界，促进了发展”。21 世纪是海洋科学的时代，由陆向海，让我们携手迈进中国海洋科学的黄金时代。

目 录

1. 冰下沉积体记录南极冰盖响应更新世晚期千年尺度气候旋回

翻译人：仲义 zhongy@sustech.edu.cn

Piccione G., Blackburn, T., Tulaczyk, S., et al. ***Subglacial precipitates record Antarctic ice sheet response to late Pleistocene millennial climate cycles*** *[J]. Nature Communications, 2022, 13(1), 5428.*

https://doi.org/10.1038/s41467-022-33009-1

摘要：冰芯和近海沉积记录表明，南极海岸边缘的海冰融化发生在末次冰川终止期内的千年尺度暖期阶段。然而，这些记录的远端位置和较短的时间覆盖范围导致了海冰损失的空间变化以及千年尺度的海冰响应是否发生在冰川末端之外的不确定性。本文作者发现了晚更新世千年尺度旋回同步的冰下沉淀物矿物学周期变化。地球化学和年代学结构提供了在寒冷时期通过冰下盐水的低温浓缩作用形成蛋白石和暖期通过增加冰盖内部冰下融水产生方解石的证据。这些冰-水循环表示由冰盖速度波动驱动的冰下水文连通性的周期性变化。研究表明，无论气候背景如何变化，南大洋地区温度振荡作用驱动了海洋的南极冰盖在千年尺度动态响应。

ABSTRACT: Ice cores and offshore sedimentary records demonstrate enhanced ice loss along Antarctic coastal margins during millennial-scale warm intervals within the last glacial termination. However, the distal location and short temporal coverage of these records leads to uncertainty in both the spatial footprint of ice loss, and whether millennial-scale ice response occurs outside of glacial terminations. Here we present a >100 kyr archive of periodic transitions in subglacial precipitate mineralogy that are synchronous with Late Pleistocene millennial-scale climate cycles. Geochemical and geochronologic data provide evidence for opal formation during cold periods via cryoconcentration of subglacial brine, and calcite formation during warm periods through the addition of subglacial meltwater originating from the ice sheet interior. These freeze-flush cycles represent cyclic changes in subglacial hydrologicconnectivity driven by ice sheet velocity fluctuations. Our findings imply that oscillating Southern Ocean temperatures drive a dynamic

response in the Antarctic ice sheet on millennial timescales, regardless of the background climate state.

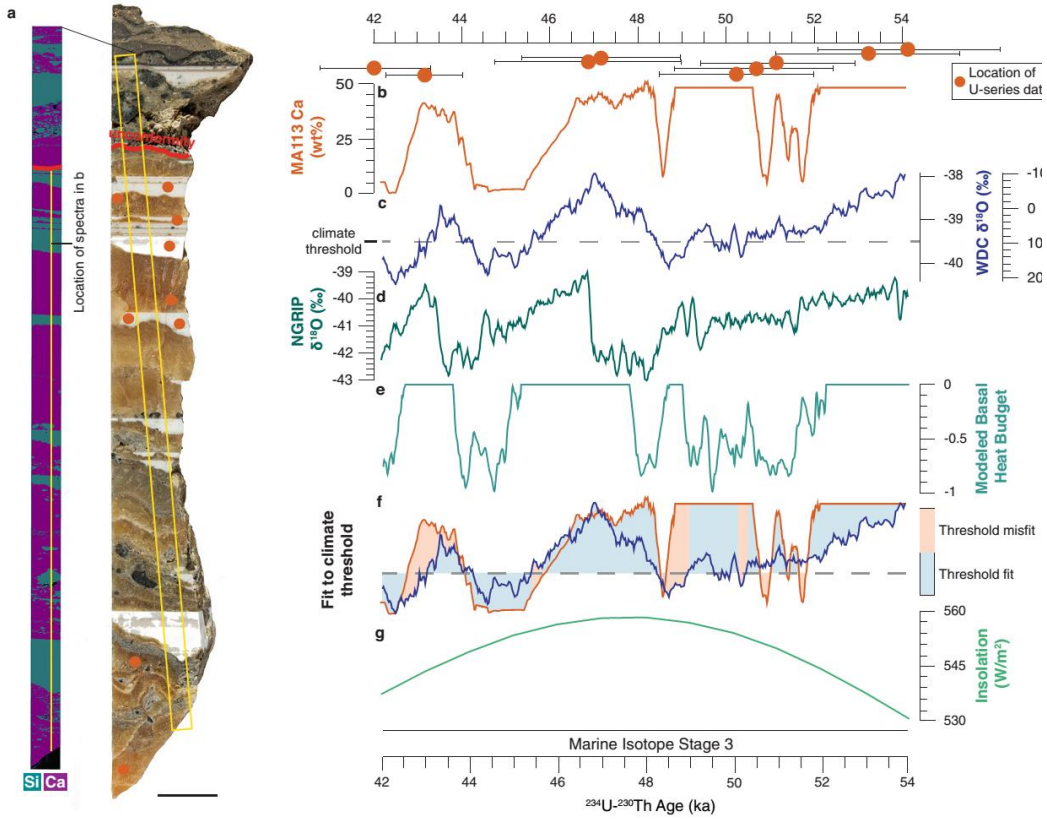

Figure 1. Sample MA113 SEM-EDS image and comparison to climate records. a Slab and SEM-EDS image of sample MA113. Scale bar is 1 cm. b Ca concentration of subglacial precipitate sample MA113. High values represent calcite precipitation; low values represent opal precipitation. U-series dates include 2σ uncertainties bars. c $\delta^{18}O$ measured in West Antarctic Divide Ice Core (WDC)107. Gray dashed line delineates threshold value for magnitude of ice thickness change necessary to elicit subglacial hydrologic response. d $\delta^{18}O$ measured in Northern Greenland Ice Core Project (NGRIP)108. e Reduced complexity model of ice sheet thermodynamics (RCMIST) output of basal heat budget over the formation timeframe of sample MA113 in units of mm/year of equivalent basal freezing rate. Negative values indicate freezing. Positive values correspond to basal melting and are truncated at 0 mm/yr. Forcing for RCMIST is provided by ice thickness changes at the foothills of the Transantarctic Mountains, which are parameterized as a linear function of the ice core isotopic record. The magnitude and scale of these thickness changes is shown on the y-axis in c. f Binary measure of fit between mineral cyclicity in b and climate threshold on WDC data in c. A

fit is defined as points where both WDC values fall above the climate threshold and calcite is precipitated, or WDC values fall below the threshold and opal is precipitates. Otherwise, the point is considered misfit. g Southern Hemisphere summer insolation (75°S) over the period of MA113 formation. The record in d is synchronized to AICC2012 chronology; the record in b is synchronized WD2014 chronology. Isotope ratios are on the VSMOW (Vienna Standard Mean Ocean Water) scale.

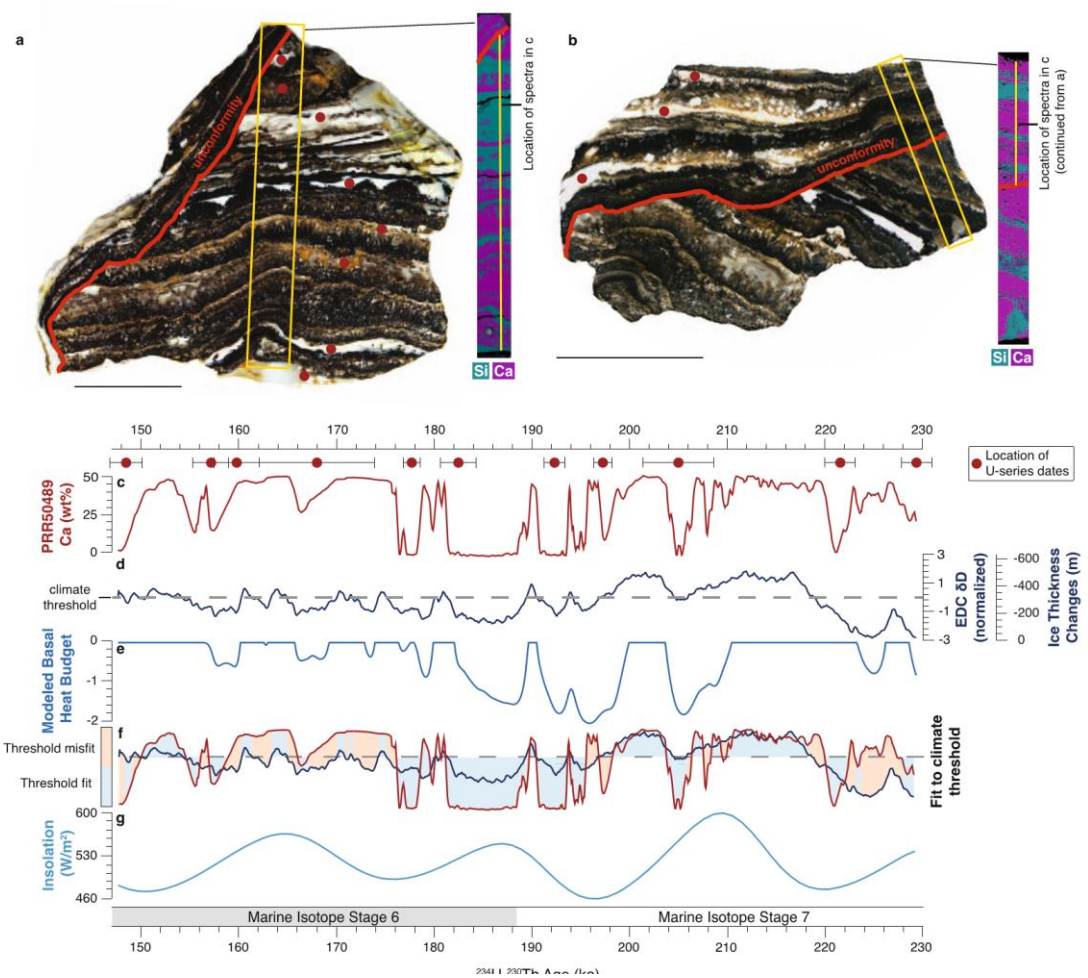

Figure 2. Sample PRR50489 SEM-EDS image and comparison to climate records. a Slab and SEM-EDS image of sample PRR50489. b Slab and SEM-EDS image of second piece of sample PRR50489. This piece of sample includes material above angular unconformity. Scale bars are 1 cm. c Ca concentration of subglacial precipitate sample PRR50489. High values represent calcite precipitation; low values represent opal precipitation. U-series dates include 2σ uncertainties bars. d δD measured in EPICA Dome C Ice Core (EDC). EDC record is detrended and converted to a z-score by zero-mean normalization to eliminate orbital trends. Gray dashed line delineates threshold

value for magnitude of ice thickness change necessary to elicit subglacial hydrologic response. e Reduced complexity model of ice sheet thermodynamics (RCMIST) output of basal heat budget over the formation period of sample PRR50489 in units of mm/year of equivalent basal freezing rate. Negative values indicate freezing. Positive values correspond to basal melting and are truncated at 0 mm/yr. Forcing for RCMIST is provided by ice thickness changes at the foothills of the Transantarctic Mountains, which are parameterized as a linear function of the ice core isotopic record. The magnitude and scale of these thickness changes is shown on the y-axis in c. f Binary measure of fit between mineral cyclicity in c and climate threshold on EDC data in d. A fit is defined as points where both EDC values fall above the climate threshold and calcite is precipitated, or EDC values fall below the threshold and opal is precipitates. Otherwise, the point is considered misfit. g Southern Hemisphere summer insolation (75°S) over the period of PRR50489 formation. Record in d is synchronized to AICC2012 chronology.

2. 热液矿床记录古海水氧同位素组成

翻译人：蒋晓东 jiangxd@sustech.edu.cn

Johnson B W., Wing B A., Abbott L. ***Hydrothermal ore deposits record the oxygen isotope composition of meteoric paleo-waters in the San Juan Volcanic Field, Colorado, USA*** *[J]. Geophysical Research Letters, 2022.*

https://doi.org/10.1029/2022GL098159

摘要：大气降水的稳定同位素比值在地形障碍上的变化是可预测的。我们提出了一种从大陆火山区热液蚀变的空间模式测定古大气降水稳定同位素比值的新方法。在美国科罗拉多州圣胡安火山区，我们重建了水的 $\delta^{18}O$ 值，在 35-20 Ma 范围内，水热液系统的 $\delta^{18}O$ 值为-7 - -10‰，随后在 20-12 Ma 范围内下降到-17 - -18‰。这一下降与更大的岩浆水输入到更古老的热液系统、或约 1.5 公里的岩石体、或约 2 - 3 公里的表面隆起，或三者的结合一致。我们的方法集成了陆地热液系统在空间（公里到 10 秒公里）和时间（10^4 - 10^6 年）尺度上的水同位素组成。这样的长度和时间尺度接近那些构造的长度和时间尺度，可能会缓解与其他古大气降水指标相关的成岩空间和时间限制的问题。

ABSTRACT: The stable isotope ratios of meteoric waters change predictably over orographic barriers. We present a new approach to determine stable isotope ratios in ancient meteoric waters from spatial patterns of hydrothermal alteration in continental volcanic fields. In the San Juan Volcanic Field, Colorado, USA we reconstruct water $\delta^{18}O$ values feeding hydrothermal systems of -7 to -10‰ from 35-20 Ma, followed by a drop to -17 to -18‰ between 20-12 Ma. This drop is consistent with greater magmatic water input to older hydrothermal systems, ~1.5 km of rock exhumation, ~2 to 3 km of surface uplift, or a combination of all three. Our approach returns water isotope compositions integrated over spatial (kms to 10s kms) and temporal (10^4– 10^6 years) scales of continental hydrothermal systems. Such length- and time-scales approach those of tectonics, potentially alleviating issues with diagenetic space and time limitations associated with other paleo-

meteoric water proxies.

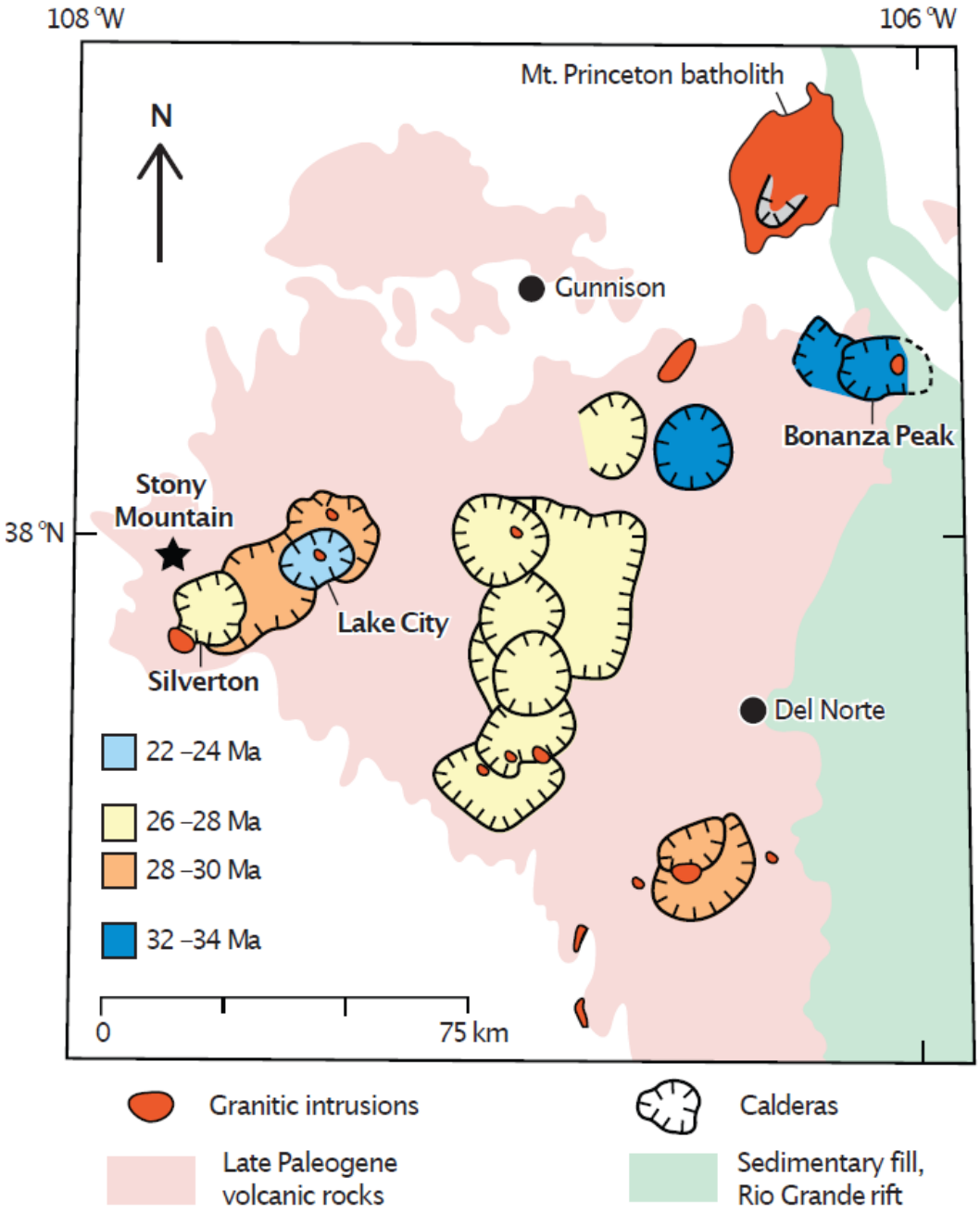

Figure 1. Simplifed geologic map (Lipman et al., 1973; Chapin, 2012; Lipman & Bachmann, 2015), showing the location and ages of calderas, and the extent of volcanic rocks, sedimentary fill, and granitic intrusions from the San Juan Volcanic Field, USA. Sites (Bonanza, Lake City, Silverton, Stony Mountain) used in this study are labeled. The region experienced broad magmatism and volcanism from the Oligocene to late Miocene, potentially related to a regional ignimbrite are-up (Chapin, 2012).

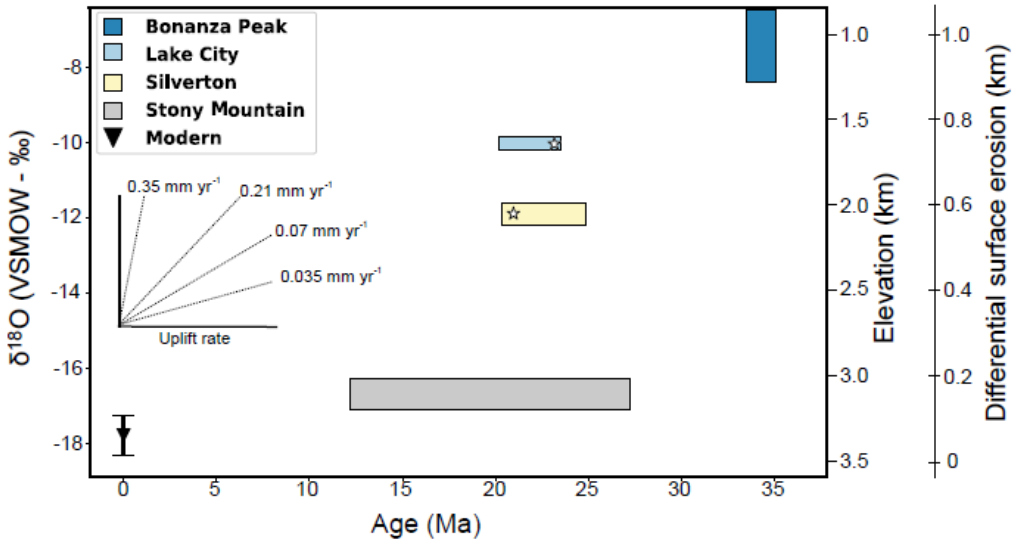

Figure 2. $\delta^{18}O$ measurements of modern surface waters (Kendall & Coplen, 2001) and new estimates of $\delta^{18}O$ in meteoric paleo-waters from sites in the SJVF (relative to V-SMOW). The height of each rectangle represents uncertainty in $\delta^{18}O$ estimates, while the width represents the full duration of magmatic activity, including caldera forming eruptions and later intrusive events (Lipman & Bachmann, 2015). The Lake City and Silverton calderas have direct geochronology on hydrothermal minerals, shown as stars. Hypothesized elevations are shown on the secondary y-axis, based on an isotope to elevation relationship of 3‰ per km (Chamberlain et al., 2012). Offset y-axis indicates thickness of dierenital erosion required to reproduce observed isotopic patterns. Inset illustrates a range of uplift rates from 0.035 to 0.35 mm yr^{-1} (Abbott et al., 1997).

3. 非光合作用植被对粉尘排放的影响

翻译人：盖聪聪 gaicc@sustech.edu.cn

Huang X., Foroutan H. ***Effects of non-photosynthetic vegetation on dust emissions*** *[J]. Journal of Geophysical Research: Atmospheres, 2022, 127, e2021JD035243.*

https://doi. org/10.1029/2021JD035243

摘要：矿物粉尘是全球气溶胶负荷的主要贡献者之一。非光合植被（NPV）抑制扬尘的能力已得到广泛认可，但尚未在区域-全球尺度的模式中进行真实表征。本文将基于卫星的植被总量数据集（包括 NPV）应用到区域大气化学模式中，并对 2016 年美国周边地区进行了模拟。为了测试粉尘模拟对 NPV 覆盖度的响应，我们进行了只包含光合植被（PV）的控制模拟。由于 NPV 的影响，美国西南部大部分地区模拟的春季到秋季粉尘排放量减少了 10%-70%。春季粉尘含量的降低程度最大，减弱了对细粒土壤浓度的过度预测，但对夏季的低估程度更高。NPV 大体上稍改善年度模拟的平均误差和相关性。NPV 主要通过遮蔽表面和通过阻力分配增加阈值速度来调节粉尘排放。此外，我们还研究了植被高度的影响，并通过一系列敏感性测试表明其不确定性。结果显示，预设植被高度 50%的改变会导致美国西南部大部分地区土壤浓度的微小变化，但会导致局部热点地区高达 30%的变化。本研究强调将 NPV 纳入沙尘模式的重要性，并指出验证总植被数据集及更真实的植被高度和季节性表示的重要性。

ABSTRACT: Mineral dust is among the top contributors to global aerosol loads. Ability of non-photosynthetic vegetation (NPV) to suppress dust emission has been widely acknowledged but a realistic representation of NPV has not been tested with regional-to-global scale models. In this study, we implemented a satellite-based total vegetation data set, which included NPV, into a regional atmospheric chemistry model and conducted simulations for the year 2016 over the conterminous United States. To test the response of dust simulations to the NPV coverage, we conducted a control simulation incorporating only the photosynthetic vegetation (PV). Simulated

dust emissions decrease by 10%–70% over most of the southwestern US from spring to autumn due to NPV. Reductions in dust concentrations are the largest in spring, which attenuate the overpredictions of fine soil concentrations, but accentuate the underpredictions in summer. Overall, the mean errors and correlations of annual simulations are slightly improved with NPV. NPV modulates dust emissions mainly by sheltering the surface and increasing the threshold velocity through drag partitioning. Moreover, we investigated the effect of vegetation height and addressed its uncertainties through a series of sensitivity tests. We observed that a 50% variation in predefined vegetation heights results in small changes in soil concentrations over majority of southwestern US, but causes up to 30% changes at local hotspots. This study highlights the significance of including NPV into the dust model and points out the importance of validation of total vegetation datasets as well as more realistic representation of vegetation heights and seasonality.

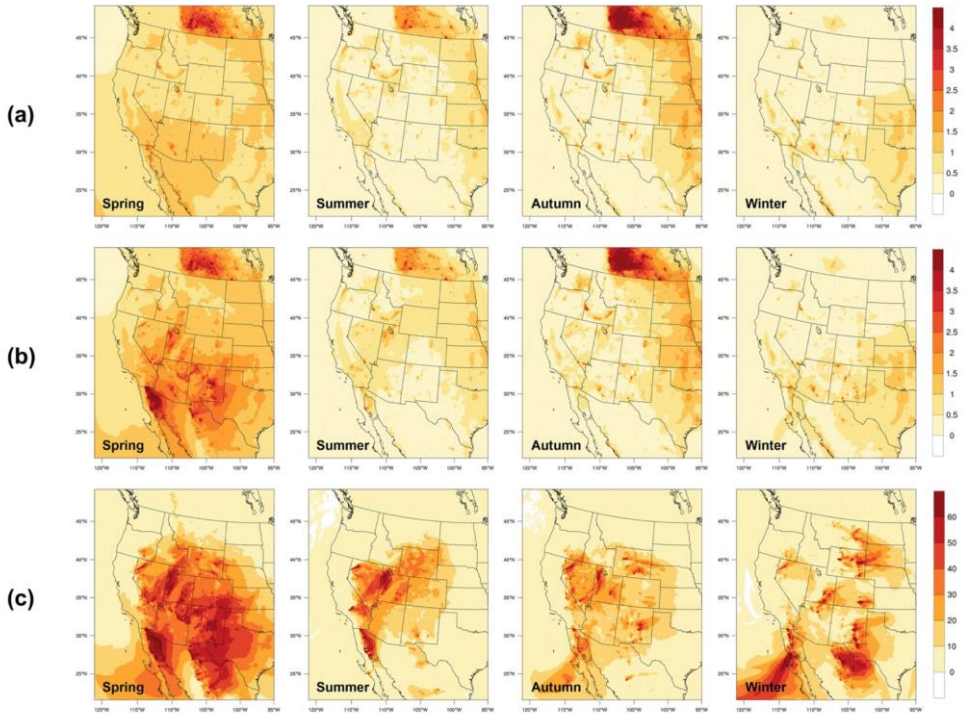

Figure 1. Seasonal averages of modeled soil concentrations (μg/m^3) over the western US from (a) the TOTAL run and (b) the fraction of absorbed photosynthetically active radiation (FPAR) run. Row (c) presents the changes in soil concentrations (%) as percentage of soil concentrations from the FPAR run after replacing the Moderate Resolution Imaging Spectroradiometer FPAR data with the total vegetation data.

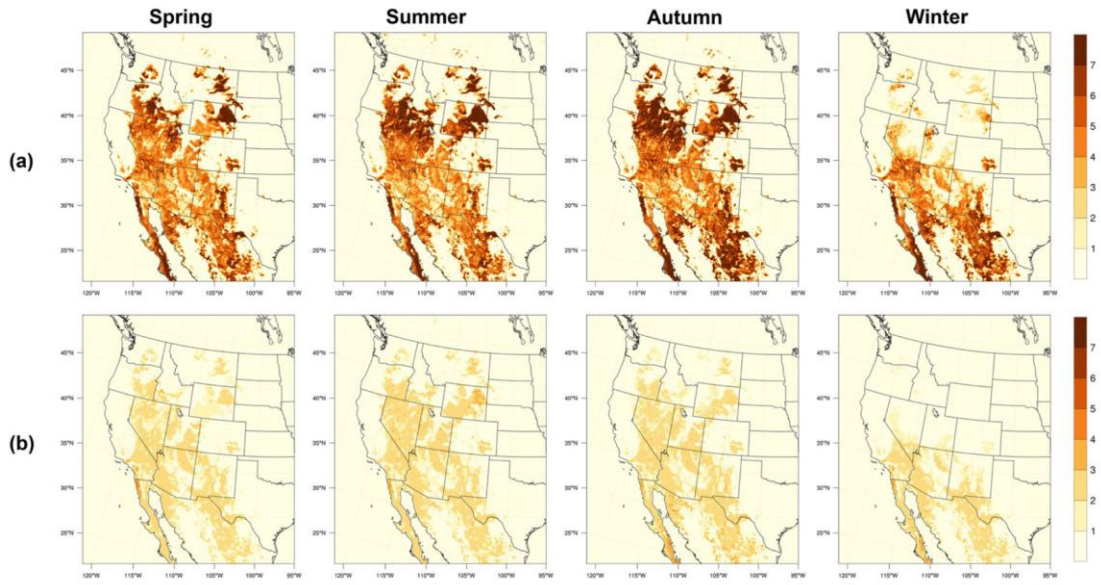

Figure 2. Seasonal averages of the roughness correction factor for the threshold velocity from (a) the TOTAL run and (b) the fraction of absorbed photosynthetically active radiation run. Values were calculated as the averages of roughness correction factors on three erodible landuse types ($f_r(L)$) weighted by the fractions of each landuse (A_L).

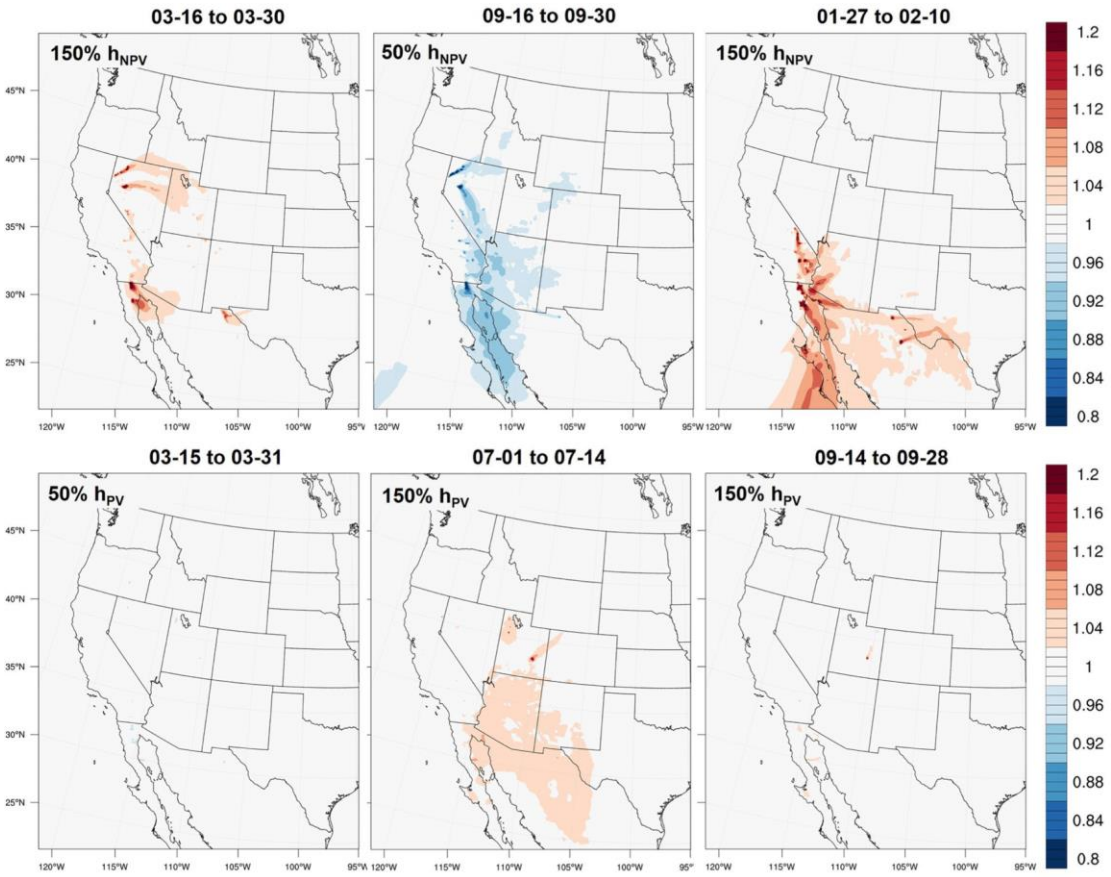

Figure 3. The ratios of simulated soil concentration from six sensitivity runs to that from the TOTAL run. The first row presents results from three sensitivity runs where heights of non-photosynthetic vegetation (NPV) were raised by 50% in spring (16–30 March) and winter (27 January–10 February), and reduced by 50% in autumn (16–30 September) in the model. The second row presents results from the other three sensitivity runs where heights of photosynthetic vegetation (PV) were reduced by 50% in spring (15–31 March) and raised by 50% in summer (1–14 July) and autumn (14–28 September). The adjusted PV and NPV heights are intended to reflect the seasonality of the average coverage of the corresponding vegetation components over the western US.

4. 端元混合分析作为湖泊沉积物记录大型风暴的探测工具

翻译人：张琪 zhangq7@sustech.edu.cn

Patterson R., Nasser N., Reinhardt E., et al. ***End-member mixing analysis (EMMA) as a tool for the detection of major storms in lake sediment records*** *[J]. Paleoceanography and Paleoclimatology, 2022.*

https://doi.org/10.1029/2022PA004510

摘要：大型热带气旋(TC)事件对北大西洋盆地西部沿海地区造成大范围的破坏。较短的仪器记录，对我们理解热带气旋长期趋势的复发与强度留下了空白，也对未来风暴发生的趋势创造了不确定性。作者对位于加拿大New Brunswick省西南部距离大西洋海岸80公里的Harvey湖长达520年的岩心记录进行了以下分析：1)湖泊沉积物粒度数据的端元混合分析（EMMA），用来确定与风暴相关的沉积过程; 2）与降水、风化、流域径流和气团相关的ITRAX XRF衍生元素比值分析（Fe、Ti、Ca/Sr、Zr/Rb、K/Rb、Br+Cl/Al）。 三个衍生端元与强降水事件（EM01）、spring freshet事件（EM02）和热带气旋事件（EM03）相关。通过对EMMA和XRF岩心数据进行CONISS分析确认了四个独特的气候带，这些气候带由不同的热带气旋的分布和降雨/风化/径流/气团来区分。在小冰期的早期，大型（EM01）降水事件和（EM03）热带气旋事件是最核心的记录特征阶段（LIAa; 区域1），大约于~1645终止。近乎停止的强降雨与热带气旋事件将随后较冷的LIAb（~1645-1825；2区）和小冰期过渡时期（约1825-1895年; 区域3）进行了区分。大约1895在LIA恢复的过程中，大型降雨和热带气旋事件再次出现。端元混合分析为识别热带气旋和大型降雨事件提供了一个强大的工具，极大地扩展了从沿海地区深入内陆进行古风暴活动研究的潜力。

ABSTRACT: Major Tropical Cyclone (TC) events cause extensive damage in coastal regions of the western North Atlantic Basin. The short instrumental record leaves significant gaps in understanding long-term trends in TC recurrence and intensity, creating uncertainty about future storm trends. Analysis of an ~520-year core record from Harvey Lake, located >80 km from the Atlantic coast in southwestern New Brunswick, Canada was carried out using: 1) End Member

Mixing Analysis (EMMA) of lake sediment grain size data to identify storm-linked sedimentological processes; and 2) ITRAX XRF derived element/ratios (Fe, Ti, Ca/Sr, Zr/Rb, K/Rb, Br+Cl/Al) associated with precipitation, weathering, catchment runoff and air masses. Three derived end members were correlated to heavy rainfall events (EM01), spring freshet (EM02), and TCs (EM03). CONISS analysis of the EMMA and XRF core data resulted in recognition of four unique climatic zones distinguished by distinct distributions of TC and rainfall/ weathering/ runoff/ and air masses. Numerous, major (EM01) rainfall events and (EM03) TC events characterized the basal core record during the early Little Ice Age (LIAa; Zone 1) phase, terminating at ~1645. A near cessation of heavy rainfall and TC events differentiated the subsequent colder LIAb (~1645-1825; Zone 2) and subsequent Little Ice Age Transition (~1825-1895; Zone 3). A resurgence of major rainfall and TC events occurred during recovery from the LIA starting in ~1895 (Zone 4). EMMA provides a robust tool for recognition of TC and major rainfall events, and greatly expands the potential for paleo-storm activity research well inland from coastal regions.

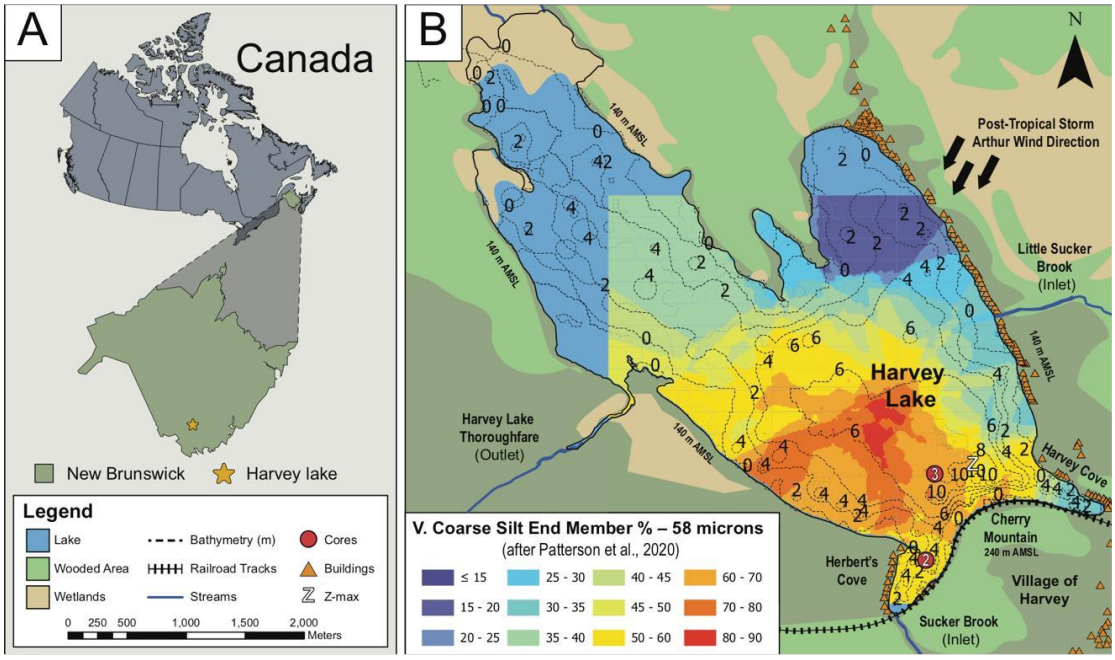

Figure 1. A. Location of Harvey Lake within Canada and Province of New Brunswick. B. An ArcGIS generated map of Harvey Lake showing area physiography, core locations used in this research, lake bathymetry, elevation relative to meters above mean sea level for the lake shore and topographic high of Cherry Mountain, and the distribution of a coarse-grained end member

determined to have been deposited in the wake of the passage of Post-Tropical Storm Arthur in July, 2014.

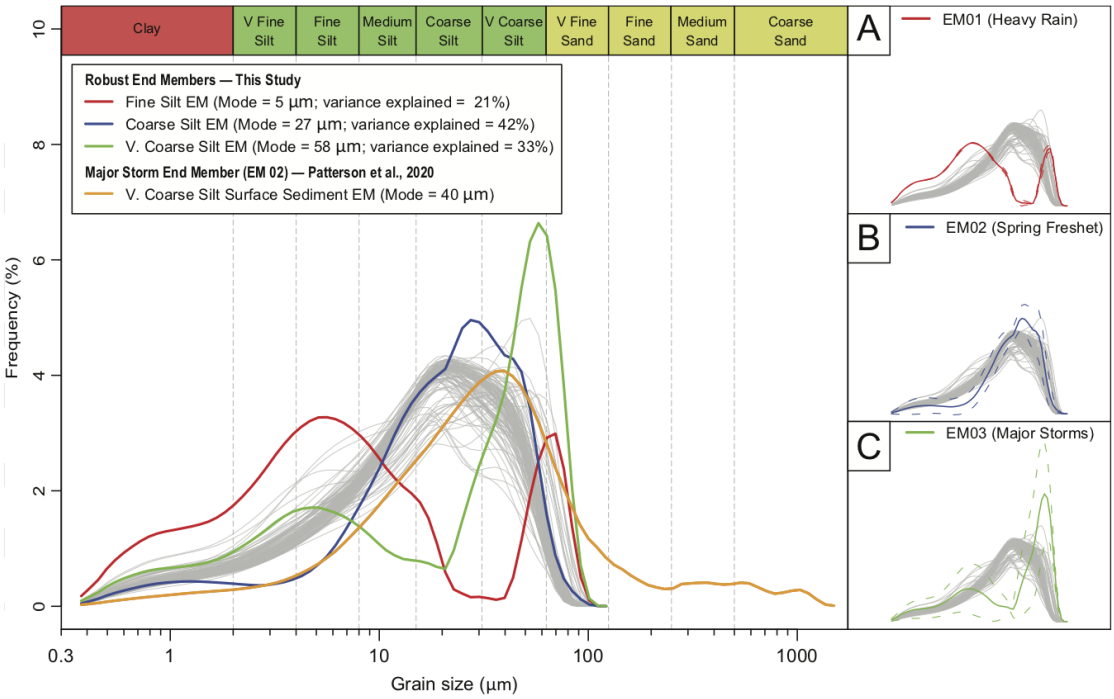

Figure 2. Grain size frequency distributions for the analyzed 115 subsamples (grey) from core HL-2017-GC-02, as well as the distribution of three derived robust end members from the selected EMMA model that best explained the sediment grain distribution in the analyzed samples. For comparison a major storm derived end member (Post-Tropical Storm Arthur), which is widely distributed across the SW part of the modern Harvey Lake bottom is plotted as an overlay.

5. 利用机器学习重建地球大气氧化历史

翻译人：张靖宇 zhangjy6@sustech.edu.cn

Chen G., Cheng Q., Lyons T W., et al. ***Reconstructing Earth's atmospheric oxygenation history using machine learning*** *[J]. Nature communications, 2022, 13(1), 1-13.*

https://doi.org/10.1038/s41467-022-33388-5

摘要：以更高的时间分辨率重建历史上的大气氧气（O_2）水平是探索地球上生命演化的首要任务。然而，这一目标受到了传统上采用的沉积物地球化学指标数据差距的挑战。在这里，我们提出了一个无监督机器学习与镁铁质火成岩地球化学大数据，以探索过去 40 亿年来的大气氧化。我们观察到大气中 O_2 的整体"两步台阶式"上升，与已发表的沉积物地球化学指标中得出的曲线相似，但叠加了 O_2 波动的更精细结构。这些额外的、短周期的波动也与先前但不太确定的关于 O_2 变化的建议一致。我们由此得出结论，地球的含氧大气至少部分可能是地幔冷却的自然结果，特别是不断演化的地幔熔体共同帮助调节了早期 O_2 来源和汇的平衡。

ABSTRACT: Reconstructing historical atmospheric oxygen (O_2) levels at finer temporal resolution is a top priority for exploring the evolution of life on Earth. This goal, however, is challenged by gaps in traditionally employed sediment-hosted geochemical proxy data. Here, we propose an independent strategy—machine learning with global mafic igneous geochemistry big data to explore atmospheric oxygenation over the last 4.0 billion years. We observe an overall two-step rise of atmospheric O_2 similar to the published curves derived from independent sediment-hosted paleo-oxybarometers but with a more detailed fabric of O_2 fluctuations superimposed. These additional, shorter-term fluctuations are also consistent with previous but less well-established suggestions of O_2 variability. We conclude from this agreement that Earth's oxygenated atmosphere may therefore be at least partly a natural consequence of mantle cooling and specifically that evolving mantle melts collectively have helped modulate the balance of early O_2 sources and sinks.

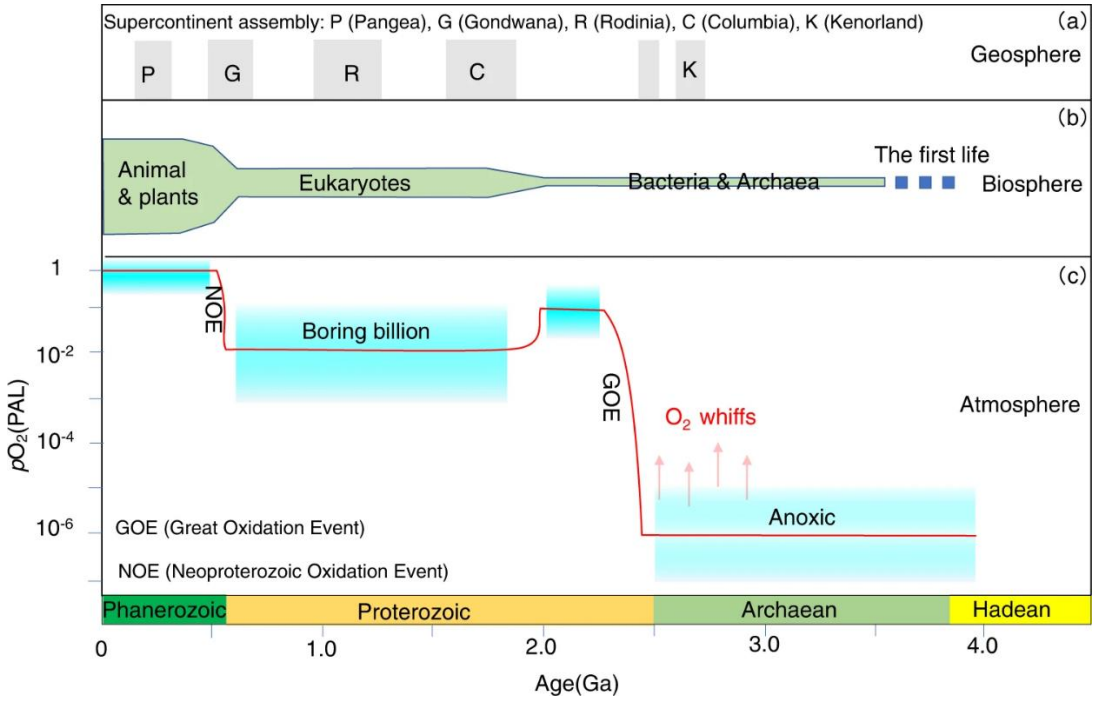

Figure 1. Co-evolution of the Earth system (geosphere, atmosphere, and biosphere) through time. a Evolution of the geosphere, including the development of the supercontinent cycles (Kenorland, Columbia, Rodinia, Gondwana, and Pangea); b Evolution of life within the biosphere; c Evolution of atmospheric oxygen levels relative to the present atmospheric level; the blue boxes show a range of atmospheric O2 level inferred from various geological proxy constraints, and the red solid line shows one plausible evolution path of O2 level.

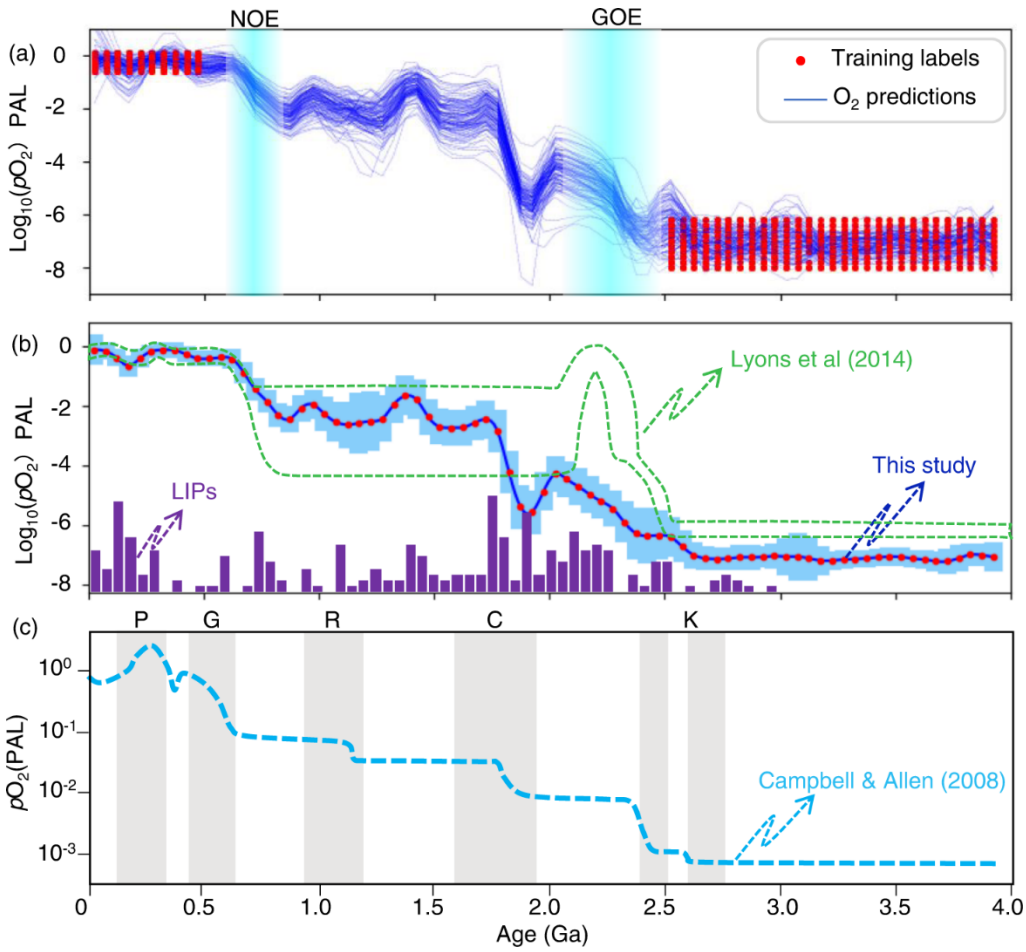

Figure 2. Quantitative prediction of atmospheric O_2 content using machine learning a All curves of support vector regression (SVR) modeling of atmospheric O_2 content using global mafic igneous geochemistry data through Monte Carlo simulations (n = 100), with random training label pairs selected pre-2.5 Ga and post-0.5 Ga. b Estimated atmospheric O_2 variation through time using mean value of 1000 simulations; the error bar shows 2 standard deviation (2-SD) uncertainties, and the green box represents the atmospheric O_2 model of Lyons et al.10. c Multistep rise model of atmospheric O_2 level proposed by Campbell and Allen, which is linked to supercontinent formations.

6. 南海边缘弧火山活动记录的古太平洋板块俯冲

翻译人：刘伟 inewway@163.com

Xu F., Zhang G., Yan W., et al. ***Subduction of the paleo-Pacific plate recorded by arc volcanism in the South China Sea margin*** *[J]. Gondwana Research, 2022, 110, 58-72.*
https://doi.org/10.1016/j.gr.2022.05.018

摘要：东亚大陆边缘的增生楔被认为是在古生代-中生代古太平洋板块俯冲作用下形成的。然而，由于幕式裂陷作用，东亚边缘的早期弧岩浆记录已被部分破坏。华南地块广泛存在的弧岩浆活动和褶皱逆冲带记录了侏罗纪和白垩纪古太平洋板块的俯冲作用。华南大陆边缘的外部在新生代发生裂谷作用形成南海，进而推测南海北部和南部存在残留弧。本研究在南海南部基于钻探 2000 米的钻孔获得了火山岩样品。岩心由玄武岩、粗面岩和少量粗面-安山岩互层组成，呈弧的微量元素分布形态。钻探岩心粗面岩锆石 U-Pb 测年结果显示，加权平均年龄为 211.2±1.6 Ma，这为东亚边缘晚三叠世火山弧的存在提供了有力证据。MgO 含量>8.5 wt% 的原始玄武岩具有最高的 εNd(i)和 εHf(i)值，表明来自印度型次弧地幔楔。玄武岩样品中 Th/Nb 的增加和 Nd−Hf 的降低表明沉积物的掺入。粗面岩样品具有丰富的 K_2O 和同位素组成，与沉积物为主的来源一致。通过与三叠纪-侏罗世板块俯冲相关的区域岩浆岩对比，认为南海南部弧火山岩记录了地幔源的在时间上的转变，代表了晚三叠世古太平洋板块俯冲的陡化。

ABSTRACT: Accretionary prisms along the East Asia continental margin have been interpreted as having formed in response to subduction of the paleo-Pacific plate in the Paleozoic–Mesozoic. However, early arc magmatic records in the East Asia margin have been partly destroyed owing to episodic rifting. Widespread arc magmatism and fold and thrust belts in the South China block have recorded Jurassic and Cretaceous paleo-Pacific plate subduction. In addition, the exterior of the South China continental margin was rifted during the Cenozoic to form the South China Sea, and it is presumed that a relic arc is preserved in the northern and southern South China Sea. In this study, we obtained samples of volcanic rocks through drilling >2000 m in the southern South China Sea.

The drill core consisted of interbedded basalts, trachytes, and minor trachy-andesites, with arc-type trace-element patterns. Zircon U–Pb dating of trachyte samples from the drill core yielded clustered ages with an overall weighted mean age of 211.2 ± 1.6 Ma, providing robust evidence for the existence of a volcanic arc in the East Asia margin during the Late Triassic. Primitive basalts with MgO > 8.5 wt% have the highest values of εNd(i) and εHf(i) and indicate derivation from Indian-type sub-arc mantle wedge. The increasing Th/Nb with decreasing Nd−Hf isotope values of the basalt samples indicates the incorporation of sediment into the melts. The trachyte samples have enriched K2O and isotopic compositions and are consistent with a sediment-dominated source. On the basis of a comparison with regional magmatic rocks related to plate subduction during Triassic–Jurassic time, the arc volcanic rocks in the southern South China Sea are interpreted to mark a temporal compositional transition in the mantle source, representing steepening subduction of the paleo-Pacific plate during the Late Triassic.

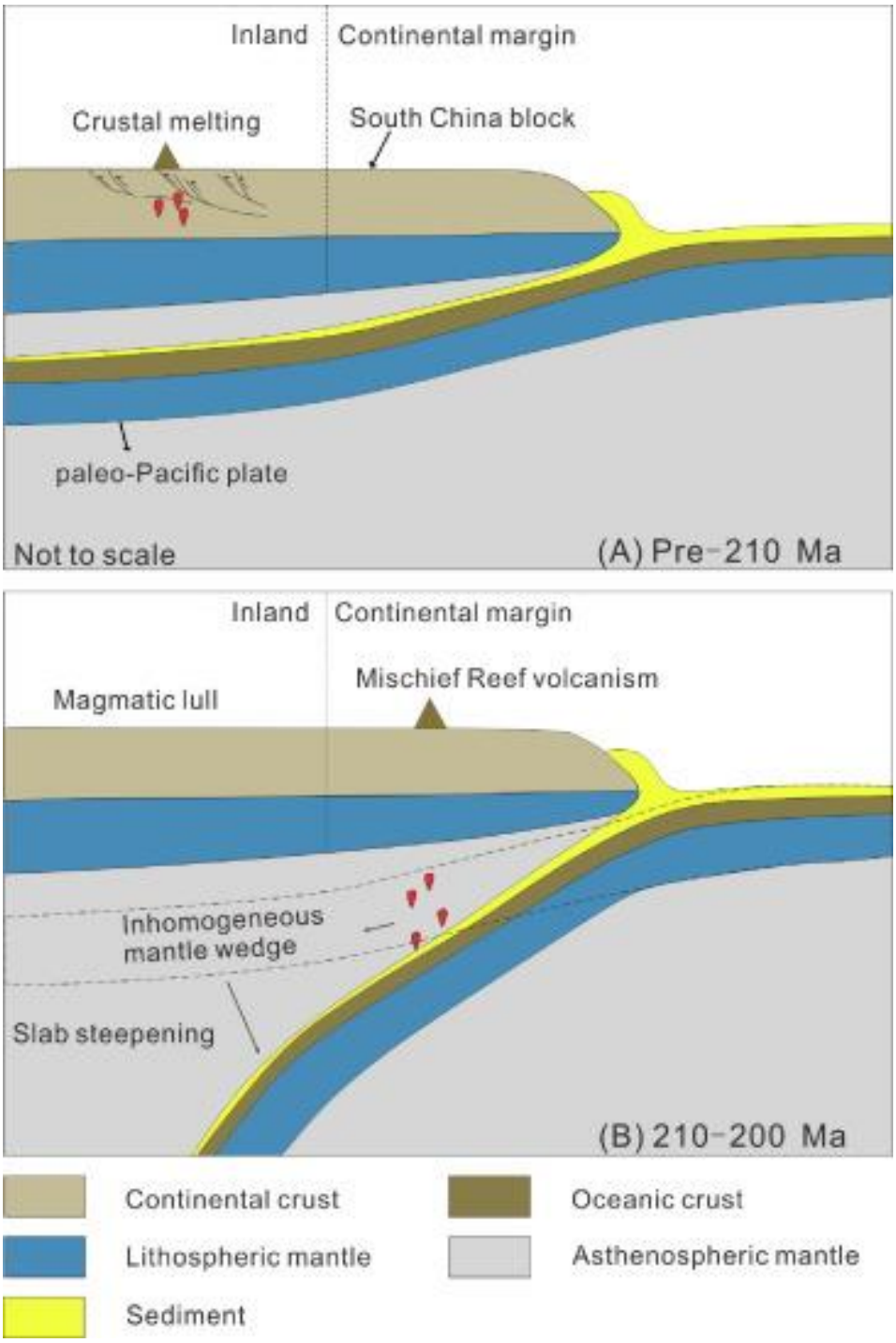

Figure 1. Tectonic evolution of the subduction of the paleo-Pacific plate beneath the South China block. (A) During the Triassic, flat subduction of the paleo-Pacific plate resulted in crustal melting in the interior of the South China block. (B) During the Late Triassic, a temporal magmatic gap in the interior of the South China block occurred as a response to the termination of flat-slab subduction. Meanwhile, Mischief Reef arc volcanism was produced in the South China continental margin as a result of slab steepening.

7. 重新解读“罗马别墅”遗址：Dračevica (Donji Radišici, Bosnia, Herzegovina)无损考古研究的第一个结果

翻译人：曹伟 11930854@qq.com

Dziurdzik T., Pisz M., Mech A., et al. ***Reinterpreting a “Roman villa” site: First results of nondestructive archaeological research in Dračevica (Donji Radišici, Bosnia, Herzegovina)*** *[J]. Archaeological Prospection, 2022, 29(3), 479-499.*

https://doi.org/10.1002/arp.1868

摘要：本文介绍了 Dračevica（Donji Radišici，Ljubuški municipality，West Herzegovina Canton，Bosnia and Herzegovina）遗址的考古勘探结果，该遗址在 19 世纪末被部分挖掘，到目前为止被解释为罗马别墅，可能具有特殊功能（路站）和一个在古代资料中得到证实的名字（Bigeste）。通过使用各种无损探测方法（航空摄影测量、野外行走测量、磁化率、磁力测量、接地电阻）、RTK GNSS 精确定位和 GIS 数据集成，对遗址进行了重新研究和解释。可以确定的是，这些建筑并不像早期研究中假设的那样是孤立的，而是一个更大的罗马定居点的一部分。研究证明，场地的内部空间划分比之前想象的更为复杂，包括沿道路分布的几个建筑群，以及土地划分系统。这样的聚落模式表明了相似的、平均大小的地块和农场。研究的重要性还在于地球物理研究的方法和成果。我们的研究是在 West Herzegovina 喀斯特地貌的罗马遗址上首次应用无损考古勘探方法，证明了该方法在这些特殊而困难的条件下的有效性。我们发现地质背景（在浅层石灰岩基岩上有一薄层低电阻的塌积土，在风化石灰岩上形成的强磁性红土）与各种仪器记录的地球物理响应之间存在相关性，即特征与其周围环境之间的磁、电对比中等至良好，地质特征异常较强。最重要的是发现特定的磁和电异常与非常浅的基岩或微弱的考古遗迹（如石灰石墙）之间的关系。我们的方法以及一些解释将有助于作为在该地区进一步调查的参考。

ABSTRACT: The article presents the results of archaeological prospection of site Dračevica (Donji Radišici, Ljubuški municipality, West Herzegovina Canton, Bosnia and Herzegovina) which was

partly excavated in the late 19th century and so far has been interpreted as a Roman villa, possibly with a special function (road station) and a name attested in ancient sources (Bigeste). Through the use of various nondestructive prospecting methods (aerial photogrammetry, fieldwalking survey, magnetic susceptibility, magnetometry, earth resistance), precise location with RTK GNSS and integration of the data in GIS, the site was restudied and reinterpreted. It was established that the structures are not isolated, as was assumed in the earlier research but rather were a part of a much larger Roman settlement. The research proves that the internal spatial division of the site is more complicated than previously thought, consisting of several building complexes located along a road, as well as land division systems. Such settlement pattern suggests similar, average-sized land plots and farms. The importance of the research lies also in the methodological approach and the outcome of the geophysical research. Our research was the first application of nondestructive methods of archaeological prospection on Roman sites in the karst landscapes of West Herzegovina, proving the usefulness of the applied methodology in these specific and difficult conditions. We have found dependencies in between the geological background (thin layer of low resistive, colluvial soil on shallow limestone bedrock and the occurrence of highly magnetic terra rossa, formed on weathered limestone) and the geophysical responses registered by various instruments, that is, moderate to good magnetic and electric contrasts between the features and their surroundings, with relatively strong anomalies from geological features. The most important was finding relationships between particular magnetic and electrical anomalies and the presence of very shallow bedrock or faint archaeological remains (e.g. limestone walls). Our methodology, as well as some of our interpretations, will be helpful as a reference for further surveys in the region.

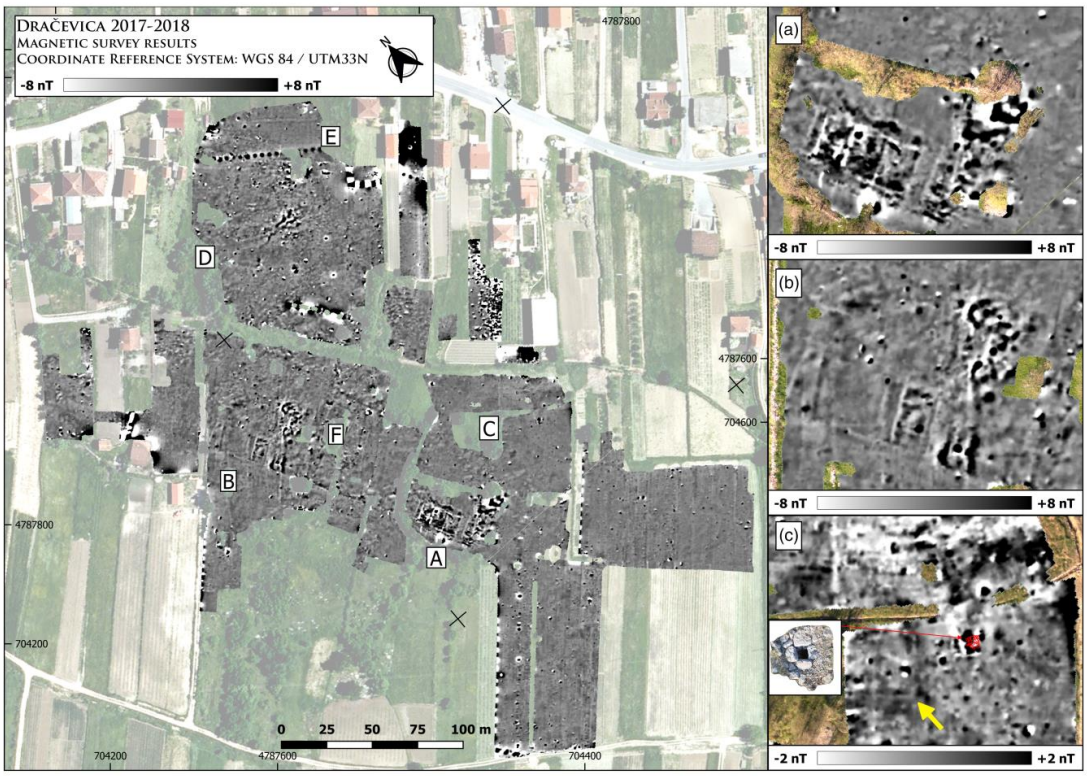

Figure 1. Magnetic survey results. General map. (a-c) Detailed views of the selected areas (please note a different dynamics scale in case of the detailed view of area C).

8. 东亚不同板块俯冲碳命运对比

翻译人：王敦繁 Dunfan-w@foxmail.com

Liu S., Wu T., Li S., et al. ***Contrasting fates of subducting carbon related to different oceanic slabs in East Asia*** *[J]. Geochimica et Cosmochimica Acta, 2022, S0016-7037(22)00125-9.*

https://doi.org/ 10.1016/j.gca.2022.03.009

摘要：俯冲作用以碳酸盐的主要形式将地表碳转移到地球内部，影响着整个地质时期的全球碳循环和地表气候。然而，在过去的俯冲带中，向下碳酸盐岩的命运是否有显著变化，很少受到自然观测的限制。海相碳酸盐相对于地幔具有较高的锌同位素比值，是俯冲碳酸盐的敏感示踪剂。本文通过对东亚南北重力线(NSGL)玄武岩的锌同位素对比研究来研究这一问题，这些玄武岩与两个不同的大洋板块有关。结合已有资料，我们发现在 NSGL 东部所有玄武岩 δ^{66}Zn 含量均较高(~ 0.3 ~ 0.6‰；N = 134)，它们不随到海沟的距离而变化，在空间上与过渡带(410-660 km)的水平停滞板耦合。这说明在古太平洋板块向西俯冲过程中，俯冲碳酸盐岩在浅溶蚀作用下存活并被深埋。而西侧玄武岩 δ^{66}Zn 随距海沟距离的增加，δ^{66}Zn 由 0.50±0.04‰逐渐下降至 0.28±0.03‰(n = 35)。目前已知的岩浆作用(如部分熔融、晶体-熔体分异、熔体-橄榄岩相互作用和脱气)无法解释 Zn 同位素的空间变化。由于这些玄武岩的地幔状铜同位素组成，也排除了来自板岩的富硫酸盐流体的作用。相反，δ^{66}Zn 的逐渐减少，以及 CaO/Al_2O_3 的耦合下降，可以解释为地幔源中溶解碳酸盐数量的减少。因此，在古亚洲板块向东南的俯冲过程中发生了大量碳酸盐溶蚀作用，从而阻止了俯冲碳的深埋。两个大板块的主要区别是: (i)与古太平洋板块相比，古亚洲板块的寿命较长(约 1.1 Ga)，扩展速度较慢，导致碳酸盐矿物主要掺入到蚀变的海洋地壳中; (ii)较年轻的古太平洋板块含有丰富的深海富镁碳酸盐，在浅层没有充分溶解。这些差异表明，不同大洋板块的俯冲作用会导致古俯冲带中俯冲碳的命运截然不同，这取决于海洋地壳中碳酸盐沉积物的含量和种类。

ABSTRACT: Subduction transfers surface carbon into the Earth's interior in a main form of carbonates that influences the global carbon cycles and surface climate through geologic time. Nevertheless, whether the fate of downgoing carbonates significantly varies in past subduction

zones is rarely constrained by natural observations. Marine carbonates have remarkably higher zinc isotopic ratios (expressed as $\delta^{66}Zn_{JMC\text{-}Lyon}$) relative to the mantle (0.99 ± 0.24‰ vs. 0.18 ± 0.05‰), making zinc isotopes a sensitive tracer for subducting carbonates. Here we examine this issue through a comparative zinc isotope study on basalts across the North-South Gravity Lineament (NSGL) in East Asia that were genetically related to two different oceanic slabs. Together with existing data, we show that all basalts in the east of the NSGL have high $\delta^{66}Zn$ (~0.3–0.6‰; n = 134) that do not vary with distances to the trench and are spatially coupled with the horizontally stagnated slab in the transition zone (410–660 km). This indicates that subducting carbonates survived shallow dissolution and were deeply buried during westward subduction of the Paleo-Pacific slab. By contrast, basalts in the west of the NSGL display a gradual decline of δ66Zn from 0.50 ± 0.04‰ to 0.28 ± 0.03‰ (n = 35) with increasing distances to the trench. No known magmatic processes (e.g., partial melting, crystal-melt differentiation, melt-peridotite interaction, and degassing) can account for the spatial Zn isotopic variation. The role of slab-derived sulfate rich fluids is also excluded because of the mantle-like Cu isotopic compositions of these basalts. Instead, the gradual decrease of δ66Zn, together with the coupled decline of CaO/Al_2O_3, are best explained as the diminished amounts of dissolved carbonates in their mantle sources. Thus, substantial carbonate dissolution must have occurred during southeastward subduction of the Paleo-Asian slab, which prevents deep burial of subducting carbon. The main differences between the two large slabs include: (i) the Paleo-Asian slab has an extended longevity (~1.1 Ga) and slow spreading rate in comparison with the Paleo-Pacific slab, leading to the main incorporation of carbonate minerals into the altered oceanic crust, and (ii) the younger Paleo-Pacific slab contains abundant deep-sea Mg-rich carbonates that were not sufficiently dissolved at shallow depths. These differences demonstrate that subduction of different oceanic slabs can lead to contrasting fates of subducting carbon in ancient subduction zones, depending on the contents and species of carbonate sediments in the oceanic crust.

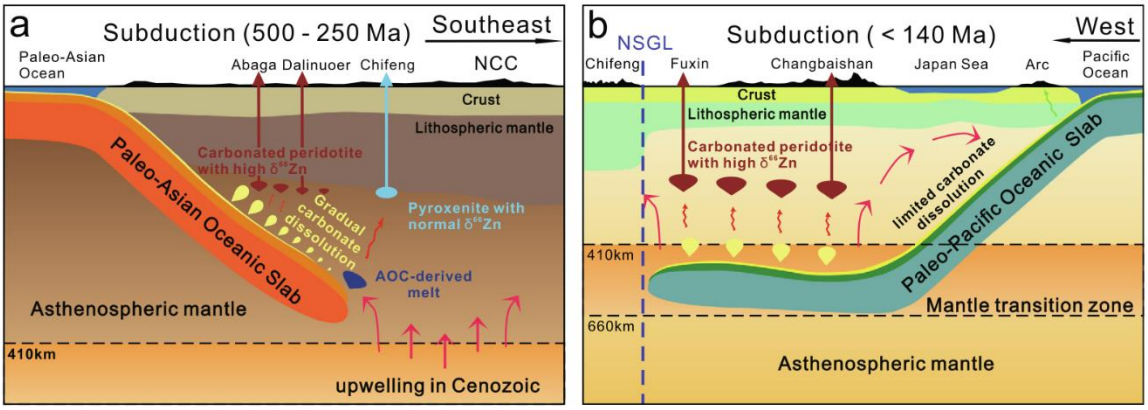

Figure 1. Schematic models showing contrasting fates of downgoing carbonates during subduction of two different oceanic slabs in East Asia. (a) Gradual dissolution of carbonates during southeastward subduction of the Paleo-Asian oceanic slab in the Paleozoic; (b) Limited dissolution at shallow depths and deep burial of carbonates during westward subduction of the Paleo-Pacific slab since the late Mesozoic.

9. 镍纹石磁畴尺寸分布

翻译人：张伟杰 12031188@mail.sustech.edu.cn

Mansbach E N., Shah J., Williams W., et al. ***Size Ranges of Magnetic Domain States in Tetrataenite*** *[J]. Geochemistry, Geophysics, Geosystems, e2022GC010631.*

https://doi.org/10.1029/2022GC010631

摘要：陨石的古磁学研究为太阳系早期磁场的演化提供了独特的约束条件。这些研究依赖于可以稳定的保持磁化超过≥45 亿年(Ga)磁性矿物。铁、石-铁和球粒陨石群中具有铁磁性矿物-镍纹石(γ″-$Fe_{0.5}Ni_{0.5}$)。虽然静磁相互作用对其剩磁获得的影响仍有待完全了解，但纳米共生的镍纹石的已被证明可以携带古磁场的信息。镍纹石也可以作为孤立的、不相互作用的纳米级颗粒出现在许多陨石群中，但是人们对这些颗粒的古地磁潜力知之甚少。本文，我们的目标是提高我们对镍纹石磁化的理解，以加深我们对现有古磁学结果的认识，并扩大可用于古磁学研究的陨石群的范围。我们呈现了对孤立存在具有不同的几何形状的镍纹石分析计算和微磁模拟结果。我们发现不同拉长程度的镍纹石颗粒在长度 6 - ~160 nm 之间形成稳定的单畴态。在 293 K 条件下，在太阳系的生命周期内它具有抵抗粘滞剩磁改造的能力。在较大的晶粒尺寸下，镍纹石的最低能态为片层双畴态，其磁化在 Ga 时间尺度上稳定。与其他磁性矿物不同的是，镍纹石由于具有较大的单轴各向异性，其不会形成单畴-vortex 畴态。研究结果表明，单畴和双畴镍纹石具有非常稳定的磁化，是一种开展古地磁研究很有前景的矿物。

ABSTRACT: Paleomagnetic studies of meteorites provide unique constraints on the evolution of magnetic fields in the early solar system. These studies rely on the identification of magnetic minerals that can retain stable magnetizations over ≥4.5 billion years (Ga). The ferromagnetic mineral tetrataenite (γ"-$Fe_{0.5}Ni_{0.5}$) is found in iron, stony-iron and chondrite meteorite groups. Nanoscale intergrowths of tetrataenite have been shown to carry records of paleomagnetic fields, although the effect of magnetostatic interactions on their magnetic remanence acquisition remains to be fully understood. Tetrataenite can also occur as isolated, non-interacting, nanoscale grains in

many meteorite groups, although the paleomagnetic potential of these grains is particularly poorly understood. Here, we aim to improve our understanding of tetrataenite magnetization to refine our knowledge of existing paleomagnetic analyses and broaden the spectrum of meteorite groups that can be used for paleomagnetic studies. We present the results of analytical calculations and micromagnetic modelling of isolated tetrataenite grains with various geometries. We find that tetrataenite forms a stable single domain state at grain lengths between 6 and ~160 nm dependent on its elongation. It also possesses a magnetization resistant to viscous remagnetization over the lifetime of the solar system at 293 K. At larger grain sizes, tetrataenite's lowest energy state is a lamellar two-domain state, stable at Ga-scale timescales. Unlike many other magnetic minerals, tetrataenite does not form a single-vortex domain state due to its large uniaxial anisotropy. Our results show that single domain and two-domain tetrataenite carries an extremely stable magnetization and therefore is a promising mineral for paleomagnetic studies.

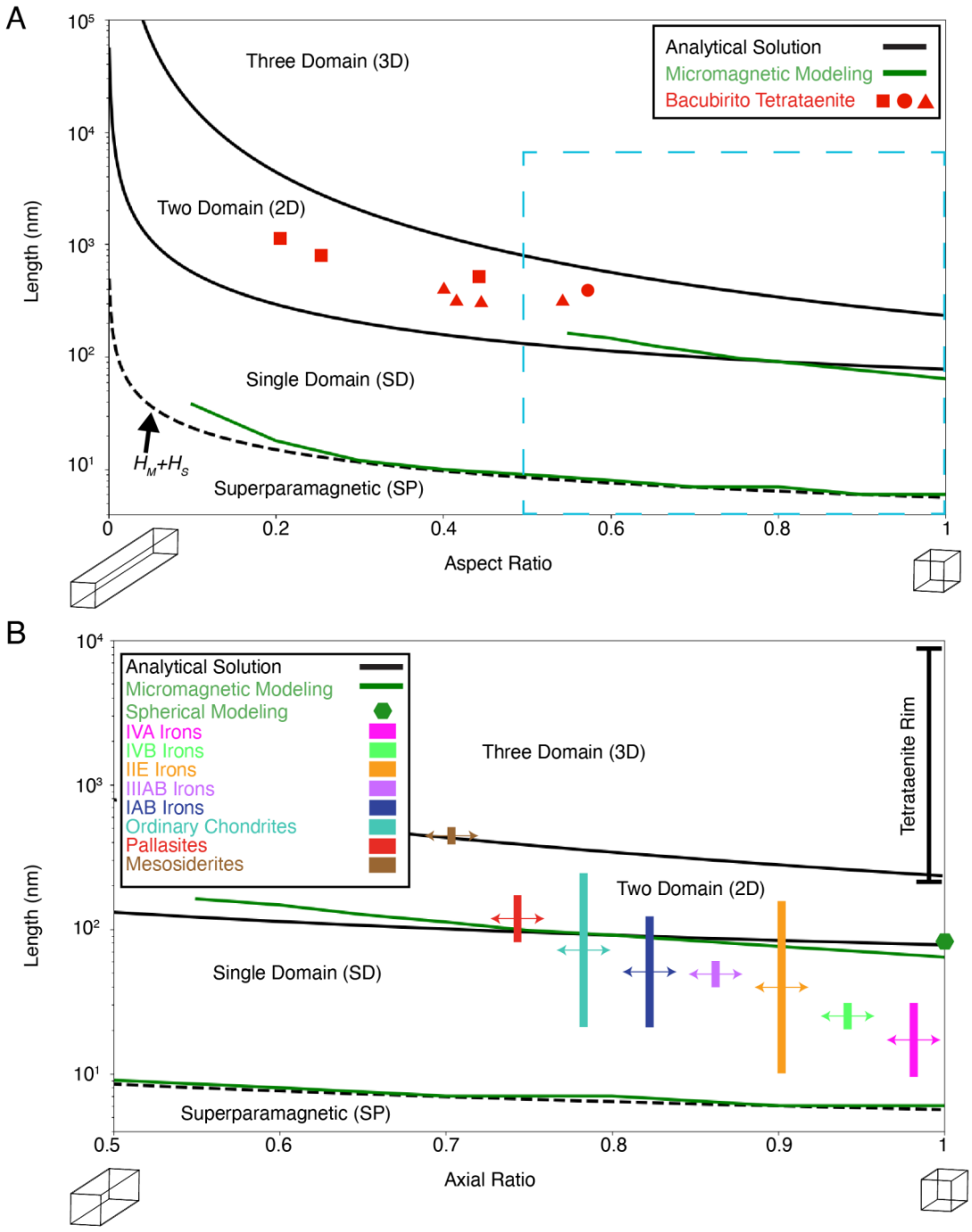

Figure 1. Domain states of tetrataenite as a function of length and axial ratio.

10. 巴西南部晚全新世古地磁方向和相对古强度记录

翻译人：李海 12031330@mail.sustech.edu.cn

Lopes C T., Savian J F., Frigo E., et al. ***Late Holocene paleosecular variation and relative paleointensity records from Lagoa dos Patos (southern Brazil)*** *[J]. Physics of the Earth and Planetary Interiors, 2022, 332, 106935.*

https://doi.org/10.1016/j.pepi.2022.106935

摘要：湖泊和泻湖沉积物是记录地磁场变化的重要载体。然而，在南半球，尤其是南美洲大陆，仅有少量的古地磁方向和相对古强度记录，这将会阻碍我们更好的理解全球的古地磁变化。此外，由于巴西南部过去几千年的古地磁记录相对匮乏，制约了我们对地球表面地磁场最弱区域的演化—南大西洋磁异常—的理解。本研究中，作者对巴西南部的帕多斯湖沉积物进行高分辨率的古地磁学及岩石磁学研究。帕多斯湖沉积物的年龄为~4540-3320 cal BP。岩石磁学结果显示主要的载磁矿物为准单畴的磁铁矿和钛磁铁矿。磁倾角和磁偏角在进行交变退磁和主成份分析后获得。PT-04 和 PT-06 孔的平均磁倾角分别为−39.6°及−38.4°。相对古强度结果与地磁场模型相一致，表明这一结果在重建这一区域的参考曲线是具有重要意义的。由于该区域在这一时期没有 PSV 和相对古强度数据，本研究将有助于理解南美过去的地磁场变化和南大西洋磁异常的演化。

ABSTRACT: Lake and lagoon sediments are important recorders of the Earth's magnetic field variations. However, the Southern Hemisphere, particularly the South American continent, contributes only a small fraction of the global paleosecular variation (PSV) and relative paleointensity data, which hinders a better understanding of the global PSV. Moreover, the scarcity of information on the geomagnetic field in South Brazil for the past few millennia impedes, for example, a detailed analysis of the evolution of the South Atlantic Magnetic Anomaly (SAMA), which encompasses the weakest geomagnetic field on the Earth's surface. Here, we present high-resolution paleomagnetic and rock magnetic data of two cores collected at the lagoon of Lagoa dos Patos, Rio Grande do Sul State, Brazil. Sediment cores from Lagoa dos Patos represent the period

from ~4540 to 3320 cal years BP. Rock magnetic results show the remanent magnetization resides in pseudo single-domain (PSD) magnetite and/or titanomagnetite. Magnetization inclinations and declinations were isolated after alternating field demagnetization (AFD) and principal component analysis (PCA). Mean inclinations are −39.6° and –38.4° for cores PT-04 and PT-06, respectively. Relative paleointensity results are compatible with geomagnetic field models, implying very promising results in the reconstruction of a reference curve for the region. As there is no PSV and relative paleointensity data for this region in this period, this study helps to elucidate the past field and the presence of SAMA in South America.

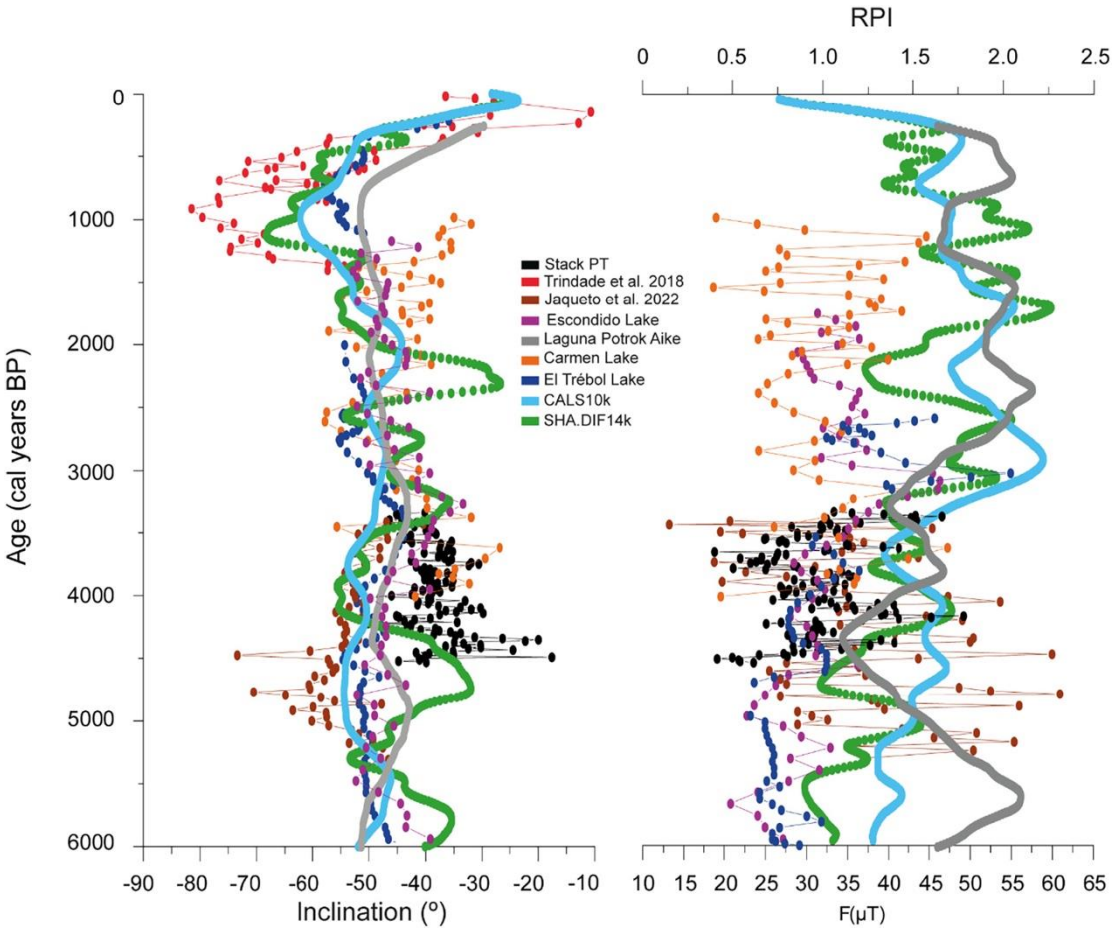

Figure 1. a) Comparison of stacked inclination logs from Carmen Lake (Gogorza et al., 2018), Potrok Aike (Gogorza et al., 2012), El Trebol (Gogorza et al., 2006), Escondido (Gogorza et al., 2004) and Lagoa dos Patos as a function of age with the models CALS10k (Brown et al., 2015; Constable et al., 2016) and SHA.DIF.14 k (Pavón Carrasco et al., 2014) outputs. We also plotted recent data from speleothem records for that same region (Trindade et al., 2018 and Jaqueto et al., 2022). And b) comparison of normalized intensity record from Lagoa dos Patos with Carmen Lake (Gogorza et al., 2018) and with relative paleointensity records from Laguna Potrok Aike (Gogorza et al., 2012), Escondido Lake (Gogorza et al., 2004), El Trébol Lake (Gogorza et al., 2006) and the models SHA.DIF14k (Pavón-Carrasco et al., 2014) and CALS10k.2 (Brown et al., 2015; Constable et al., 2016). We also plotted recent data from speleothem records for that same region (Trindade et al., 2018 and Jaqueto et al., 2022). The lower x scale is referring to absolute paleointensity data while the upper scale is referring to relative paleointensity data. (For interpretation of the references to colour in this figure legend, the reader is referred to the web version of this article.)

11. 中纬度海洋水合物分解对大气甲烷释放可以忽略不计

翻译人：张亚南 zhangyn3@mail.sustech.edu.cn

Joung D., Ruppel C., Southon J., et al. ***Negligible atmospheric release of methane from decomposing hydrates in mid-latitude oceans*** *[J]. Nature Geoscience, 2022.*

https://doi.org/10.1038/s41561-022-01044-8

摘要：天然气水合物可能对全球变暖起到积极的反馈作用，因为它们封存着大量的强温室气体—甲烷，并在海洋/大气温度上升时变得不稳定。大多数水合物存在于海洋沉积物中；由于海底水合物分解或其他甲烷池产生的气体能够造成冷泉区甲烷的泄露。不管甲烷泄露的来源如何，之前对冷泉区排放甲烷的所有测量都表明，与其他来源相比，冷泉区甲烷具有独特的化石放射性碳特征。文中，作者提供了沿美国大西洋和太平洋边缘，从冷泉区海底到海表水体中的甲烷浓度和天然放射性碳含量。在海底水合物不稳定的区域，对于较浅的水体，确实记录到了甲烷泄露。然而，对沿美国大西洋边缘的深水区测量表明，当水深大于 430± 90 m 时，没有证据表明甲烷泄漏到海表。该区域仅在水深大于-550 m 处存在天然气水合物，表明进入大气的甲烷来源并非水合物分解。

ABSTRACT: Naturally occurring gas hydrates may contribute to a positive feedback for global warming because they sequester large amounts of the potent greenhouse gas methane in ice-like deposits that could be destabilized by increasing ocean/atmospheric temperatures. Most hydrates occur within marine sediments; gas liberated during the decomposition of seafloor hydrates or originating with other methane pools can feed methane emissions at cold seeps. Regardless of the origin of seep methane, all previous measurements of methane emitted from seeps have shown it to have a unique fossil radiocarbon signature, contrasting with other sources of marine methane. Here we present the concentration and natural radiocarbon content of methane dissolved in the water column from the seafloor to the sea surface at seep fields along the US Atlantic and Pacific margins. For shallower water columns, where the seafloor is not within the hydrate stability zone, we do document seep CH4 in some surface-water samples. However, measurements in deeper water

columns along the US Atlantic margin reveal no evidence of seep CH4 reaching surface waters when the water-column depth is greater than 430 ± 90 m. Gas hydrates exist only at water depths greater than ~550 m in this region, suggesting that the source of methane escaping to the atmosphere is not from hydrate decomposition.

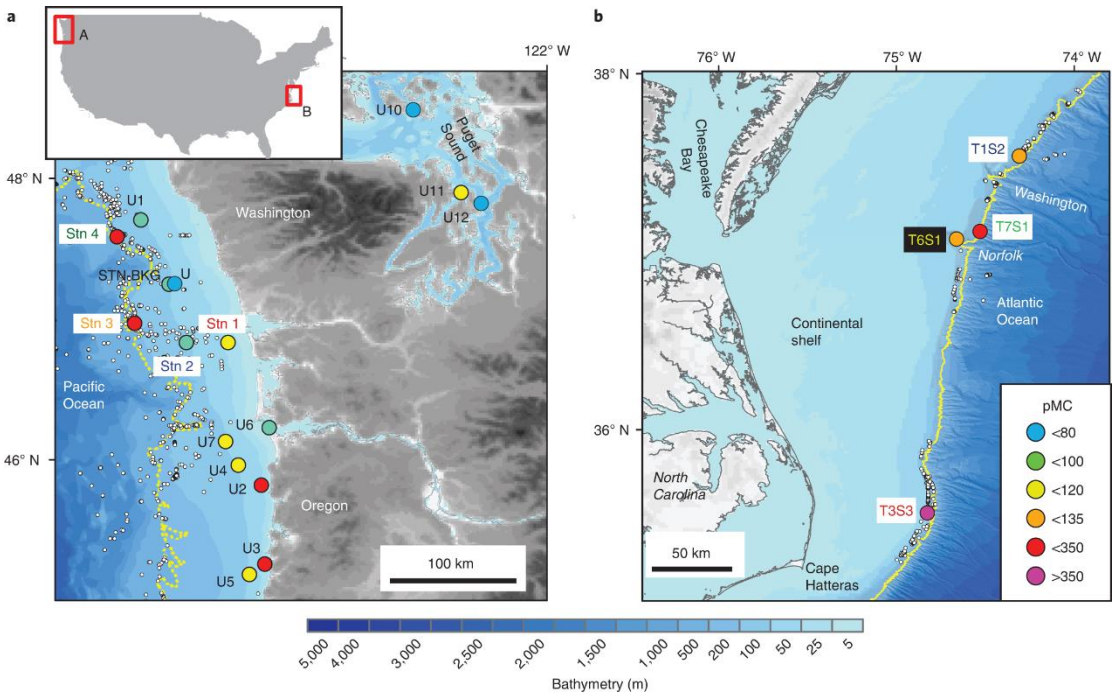

Figure 1. Summary of surface-water ^{14}C–CH_4 results. a,b, Results with units of pMC collected from near-surface waters in the Pacific Northwest (a) and the Mid-Atlantic Bight (b), in areas A and B, respectively, highlighted by the red boxes on the inset map. Salish Sea connects waters from the Pacific Ocean and Puget Sound, located between Washington, USA, and Vancouver Island, Canada, in a. Known seep locations are shown as white circles. Yellow curves indicate the approximate landward limit of gas hydrate as determined from near-bottom temperature measurements for the Pacific Northwest and corresponding to the 550 m isobath on the Mid-Atlantic margin. Note that Phrampus reported the hydrate stability depth as 480 m in Cascadia margin, Pacific Ocean. Station labels are colour coded to match those in Figs. 2 and 3.

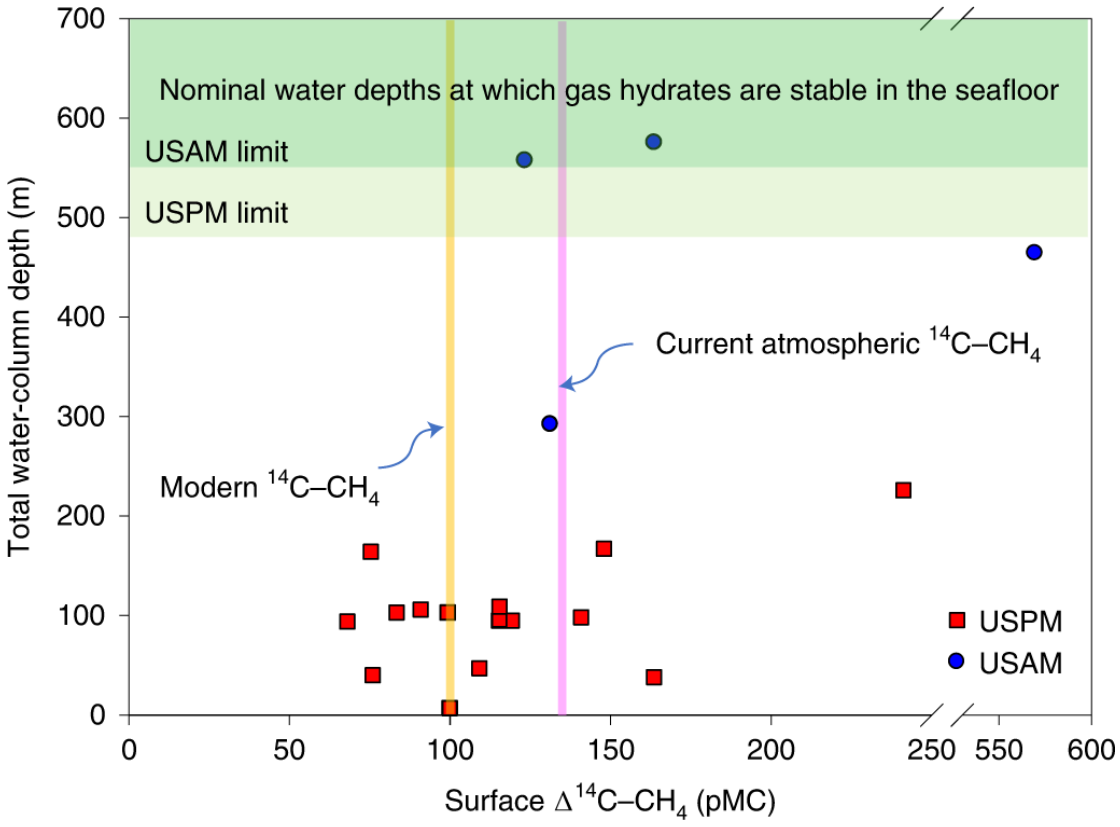

Figure 2. Plot of $^{14}C–CH_4$ dissolved in surface waters versus total water-column depth where the samples were collected. This figure displays that no surface-water samples display fossil CH_4, or any CH4 with a $^{14}C–CH_4$ value below the contemporary atmosphere or modern carbon, until the total water-column depth is less than or equal to 164 m.

12. 古新世-始新世极热期气候变化的空间格局

翻译人：夏文月 12231072@mail.sustech.edu.cn

Jessica E T., Zhu J., Li M., et al. ***Spatial patterns of climate change across the Paleocene-Eocene Thermal Maximum*** *[J]. PNAS, 2022, 119(42), 1–7.*

https://doi.org/10.1073/pnas.2205326119

摘要：古新世-始新世极热期（PETM：56Ma）是理解 "温室 "世界中气候动态的最佳地质类比物之一。然而代表这一事件的替代性数据仅能从不均衡地分布在地球表面的海洋和陆地沉积环境中获取，这限制了我们对气候变化空间模式的看法。在此，我们使用古气候数据同化（DA）来结合气候模型和代理指标，并在空间上完整重建 PETM 和它之前的气候状态（"PETM-DA"）。我们数据受限的结果支持强烈的极地增强作用，在缺乏大面积冰冻层的情况下，这与温度反馈和陆地上季节性降雪的损失有关。水文循环对 PETM 变暖的响应包括热带辐合带的变窄、赤道外的干燥以及季节性季风和冬季风暴路径的加强。其中许多特征也可以在模拟未来人类排放量增加的情况下的气候变化中看到。由于 PETM-DA 产生了空间上完整的地表空气温度估计，它得出了严谨的全球平均温度变化估计（5.6 °C；5.4°C-5.9 °C，95% CI），可用于计算平衡气候敏感度(ECS)。我们发现 PETM 的 ECS 为 6.5 °C（5.7 °C-7.4 °C，95% CI），远远高于现今的幅度。这支持了当温室气体浓度高时，气候敏感度会显著增加的一种观点。

ABSTRACT: The Paleocene-Eocene Thermal Maximum (PETM; 56 Ma) is one of our best geological analogs for understanding climate dynamics in a "greenhouse" world. However, proxy data representing the event are only available from select marine and terrestrial sedimentary sequences that are unevenly distributed across Earth's surface, limiting our view of the spatial patterns of climate change. Here, we use paleoclimate data assimilation (DA) to combine climate model and proxy information and create a spatially complete reconstruction of the PETM and the

climate state that precedes it ("PETM-DA"). Our data-constrained results support strong polar amplification, which in the absence of an extensive cryosphere, is related to temperature feedbacks and loss of seasonal snow on land. The response of the hydrological cycle to PETM warming consists of a narrowing of the Intertropical Convergence Zone, off-equatorial drying, and an intensification of seasonal monsoons and winter storm tracks. Many of these features are also seen in simulations of future climate change under increasing anthropogenic emissions. Since the PETM-DA yields a spatially complete estimate of surface air temperature, it yields a rigorous estimate of global mean temperature change (5.6 °C; 5.4°C to 5.9 °C, 95% CI) that can be used to calculate equilibrium climate sensitivity (ECS). We find that PETM ECS was 6.5 °C (5.7 °C to 7.4 °C, 95% CI), which is much higher than the present-day range. This supports the view that climate sensitivity increases substantially when greenhouse gas concentrations are high.

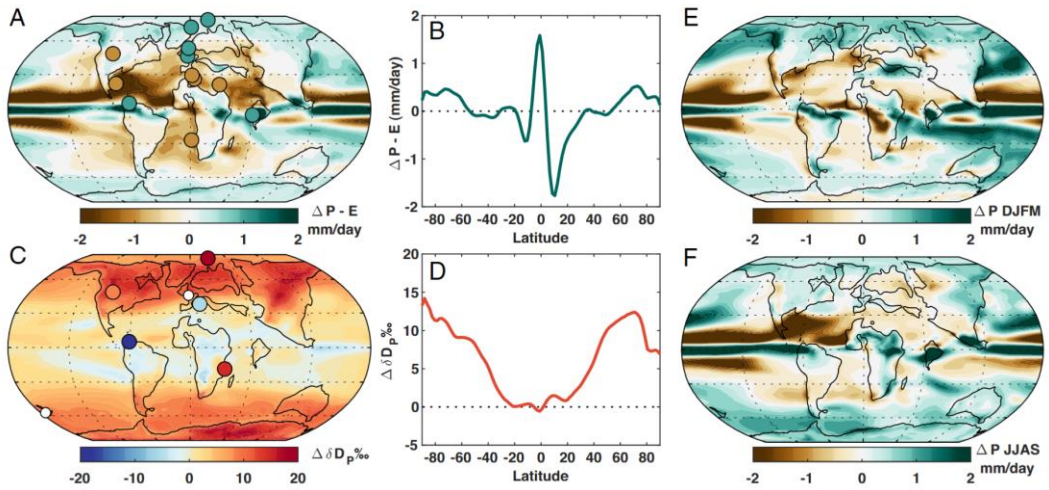

Figure 1. Changes in the hydrological cycle during the PETM. All panels represent PETM - pre-PETM anomalies. (A) Change in mean annual precipitation minus evaporation (P - E) in the PETM-DA overlain with proxy indicators for relatively wetter (green) or drier (brown) conditions relative to the pre-PETM. Proxy data are from the compilation of ref. 12 with the addition of data from ref. 34 (SI Appendix). Proxy colors are qualitative and indicate the sign of change only. (B) Zonal mean annual change in P - E. (C) Change in the mean annual δD of precipitation (δDp) in the PETM-DA overlain with inferred changes from leaf wax δD (Dataset S2). Sites with significant changes during the PETM are colored on the same scale as the DA results; sites without significant changes are

plotted as smaller white dots. (D) Zonal mean annual change in δDp. (E) The December to March (DJFM) change in precipitation (△P). (F) The June to September (JJAS) change in precipitation.

13. 格陵兰岛冰川的海底融化被大气变暖所放大

翻译人：刘宇星 liuyx2018@mail.sustech.edu.cn

Slater D A., Straneo F. ***Submarine melting of glaciers in Greenland amplified by atmospheric warming*** *[J]. Nature Geoscience, 2022, 1-6.*

https://doi.org/10.1038/s41561-022-01035-9

摘要：自 1992 年以来，格陵兰岛冰盖的快速失冰是由于表面融化的增加和冰流的加速造成的。后者传统意义上被归因于海洋变暖，这加强了格陵兰海洋冰川前沿的海底融化。这是通过将冰架表面的融水释放到海洋中，激发冰川附近的海洋循环，进而将热量从海洋转移到冰盖上，这意味着即使没有海洋变暖，大气变暖也会增加海底融化。然而，大气和海洋变暖在推动海底融化增加方面的相对重要性还没有被量化。在这里，我们重建了 1979 年至 2018 年格陵兰岛海洋终结冰川的海底融化率，并估计了由此产生的动态质量损失。我们表明，在格陵兰岛南部，海冰底部融化的变化确实受海洋的支配，但与此相反，在西北部则由大气主导。在冰架规模上，大气在控制海底融化和随后的动态质量损失方面起着一阶作用。我们的结果挑战了将动态质量损失仅仅归因于海洋变暖的观点，并表明大气变暖放大了海洋对格陵兰冰盖的影响。

ABSTRACT: Rapid ice loss from the Greenland ice sheet since 1992 is due in equal parts to increased surface melting and accelerated ice flow. The latter is conventionally attributed to ocean warming, which has enhanced submarine melting of the fronts of Greenland's marine-terminating glaciers. Yet, through the release of ice sheet surface meltwater into the ocean, which excites near-glacier ocean circulation and in turn the transfer of heat from ocean to ice, a warming atmosphere can increase submarine melting even in the absence of ocean warming. The relative importance of atmospheric and oceanic warming in driving increased submarine melting has, however, not been quantified. Here, we reconstruct the rate of submarine melting at Greenland's marine-terminating glaciers from 1979 to 2018 and estimate the resulting dynamic mass loss. We show that in south Greenland, variability in submarine melting was indeed governed by the ocean, but, in contrast, the

atmosphere dominated in the northwest. At the ice sheet scale, the atmosphere plays a first-order role in controlling submarine melting and the subsequent dynamic mass loss. Our results challenge the attribution of dynamic mass loss to ocean warming alone and show that a warming atmosphere has amplified the impact of the ocean on the Greenland ice sheet.

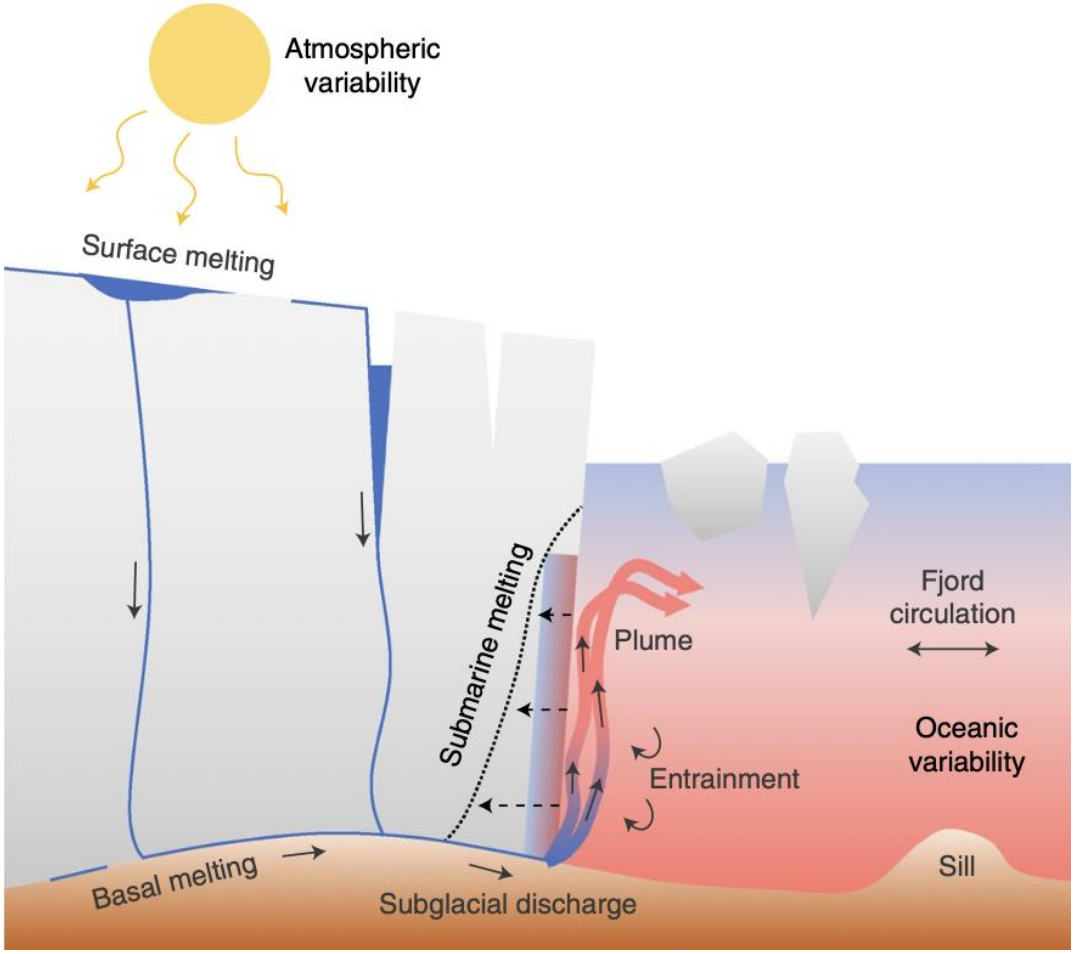

Figure 1. Submarine melting of marine-terminating glaciers influenced by both atmospheric and oceanic variability. Freshwater emerging from beneath marine-terminating glaciers (subglacial discharge) drives vigorous upwelling plumes. Subglacial discharge can be sourced either from surface melting or frictional melting at the bed. Plumes entrain warm fjord waters, which are replenished by the ocean and fjord circulation processes. The combination of fast-moving and warm water in the plume drives melting of submerged ice at the glacier terminus (submarine melting). By the described chain of processes, submarine melting is influenced by both atmospheric and oceanic variability.

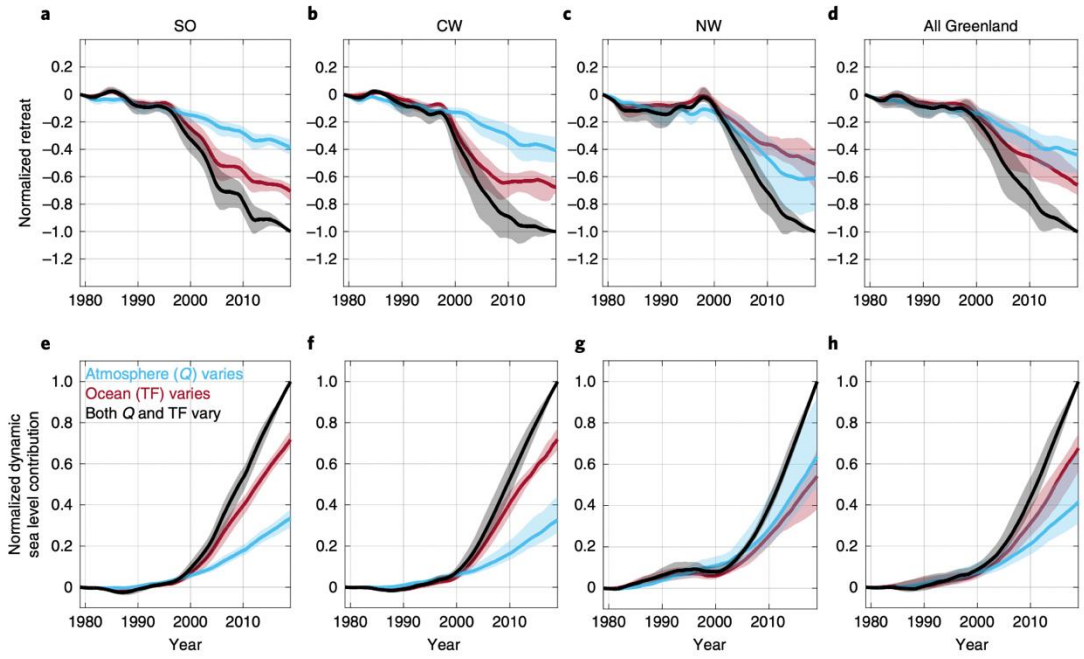

Figure 2. Relative importance of atmospheric and oceanic variability to Greenland marine-terminating glacier retreat and dynamic mass loss. a–h, The results are obtained by forcing a simple glacier model ensemble with the submarine melt rate variability shown in Fig. 3. Each plot contains the scenario in which only the atmosphere varies (blue), only the ocean varies (red) and both vary (black) for SO (a, e), CW (b, f), NW (c, g) and all Greenland (d, h). The results are normalized by the retreat (a–d) or sea level contribution (e–h) by 2018 when both atmosphere and ocean vary. The shading shows the interquartile range of results obtained by varying parameters in the model, while the solid lines show the ensemble median. The retreat and sea level time series have been smoothed using four- and one-year windows, respectively. Additional plots showing the regions not highlighted here, retreat observations and ice discharge are given in Extended Data Figs. 7-9.

14. 大陆循环在跨大陆架泥沙运输中被忽视的作用:对古气候重建的影响

翻译人：聂美娟 12232216@mail.sustech.edu.cn

Shi Y., Xu X., Sheng H., et al. ***Neglected role of continental circulation in cross-shelf sediment transport: Implications for paleoclimate reconstructions*** *[J]. Marine Geology, 2022, 443, 106703.*
https://doi.org/10.1016/j.margeo.2021.106703

摘要：沿岸海流在调节沿岸泥沙输送中起着关键作用，并且它们与冬季风暴 (东亚冬季风爆发) 和中国东部陆架沿海泥质沉积物形成的关系已被建立，在此基础上，东亚冬季风的演变也已被广泛探索。与沿岸沉积不同，中国东部陆架近海沉积的形成非常复杂且争议很大，这给基于这些沉积的古气候重建带来了巨大挑战。在本研究中，利用来自黄海北部 (NYS) 的遥感图像和沉积记录（地震剖面和沉积物粒度）探索了黄海暖流 (YSWC) 下的沉积物输送。结果表明，虽然北半球西部近海泥沙沉积是由冬季风暴触发山东半岛附近海岸沉积物搬运的形成的，但冬季风暴信号完全被黄海暖流所遮蔽，这可能决定了千年尺度上的搬运通量。在 2.8 ka 后的泥沙中还可观察到 1500 y 亚轨道气候变化周期。通过比较黄海北部同一泥质沉积物内部和相邻泥质沉积物之间的沉积物组成，我们发现泥沙输送对 YSWC 的响应在空间上是不同的，这可能是在中国东部陆架以往冬季季风重建中观察到差异的一个解释原因。因此，本研究表明，中国东部陆架近海沉积物不适合冬季风的逆温。此外，中国东部陆架的泥质沉积还受到台风和河流洪水等其他动力因素的显著影响；因此，深入探讨这些沉积物的动力学特征和形成机制是重建古气候的前提条件。

ABSTRACT: Coastal currents play a key role in regulating alongshore sediment transport, and their relationships with winter storms (burst of the East Asian winter monsoon) and formation of the coastal mud deposits on the eastern China shelf have been established, based on which the evolution of the East Asian winter monsoon has been widely explored. Unlike that of coastal deposits, the formation of offshore deposits on the eastern China shelf is very complex and highly debated,

leading to enormous challenges on paleoclimate reconstructions based on these deposits. In this study, cross-front sediment transport under a variable Yellow Sea Warm Current (YSWC) was explored using remote sensing imagery and sedimentary records (seismic profile and sediment grain size) from the North Yellow Sea (NYS). The results indicate that, although the offshore mud deposit in the western NYS is formed by winter storms through triggering cross-front transport of coastal sediment around the Shandong Peninsula, the winter storm signal was completely obscured by that of the YSWC, which might determine the flux of cross-front sediment transport on a millennial scale. The 1500 y sub-orbital climate variability cycle could also be observed in distal muds after 2.8 ka. By comparing the sediment composition within the same mud deposit or between adjacent mud deposits in the NYS, we found that the response of cross-front sediment transport to the YSWC varied spatially, which may be a reason for discrepancies observed in previous winter monsoon re-constructions on the eastern China shelf. Therefore, as indicated by this study, offshore deposits on the eastern China shelf are not suitable for inversions of the winter monsoon. In addition, mud deposits on the eastern China shelf are also dramatically affected by other dynamic factors, including typhoons and river flooding; thus, deeply exploring the dynamic characteristics and formation mechanism of these deposits are prerequisites for paleo-climate reconstruction.

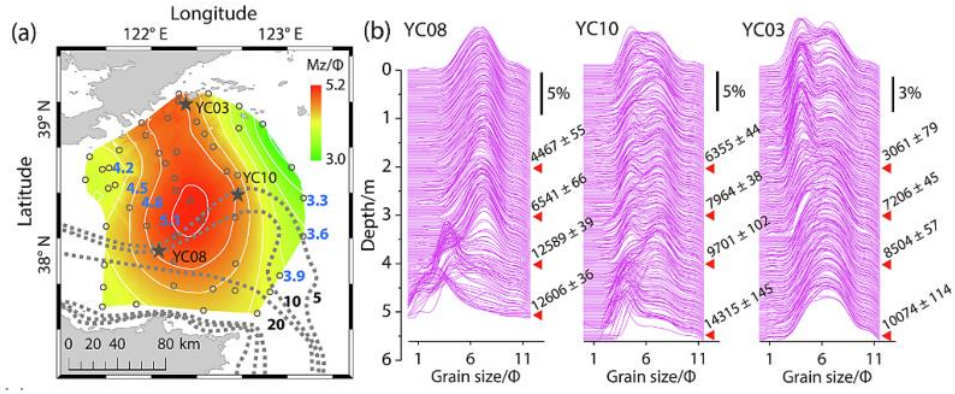

Figure 1. (a) Mean grain size distribution of the surface sediments. White lines are contour lines of the mean grain size, dotted lines are the isopachs of the mud patches around the Shandong Peninsula (Yang and Liu, 2007). (b) Grain size-frequency distributions of the sediment cores, along with the calibrated.

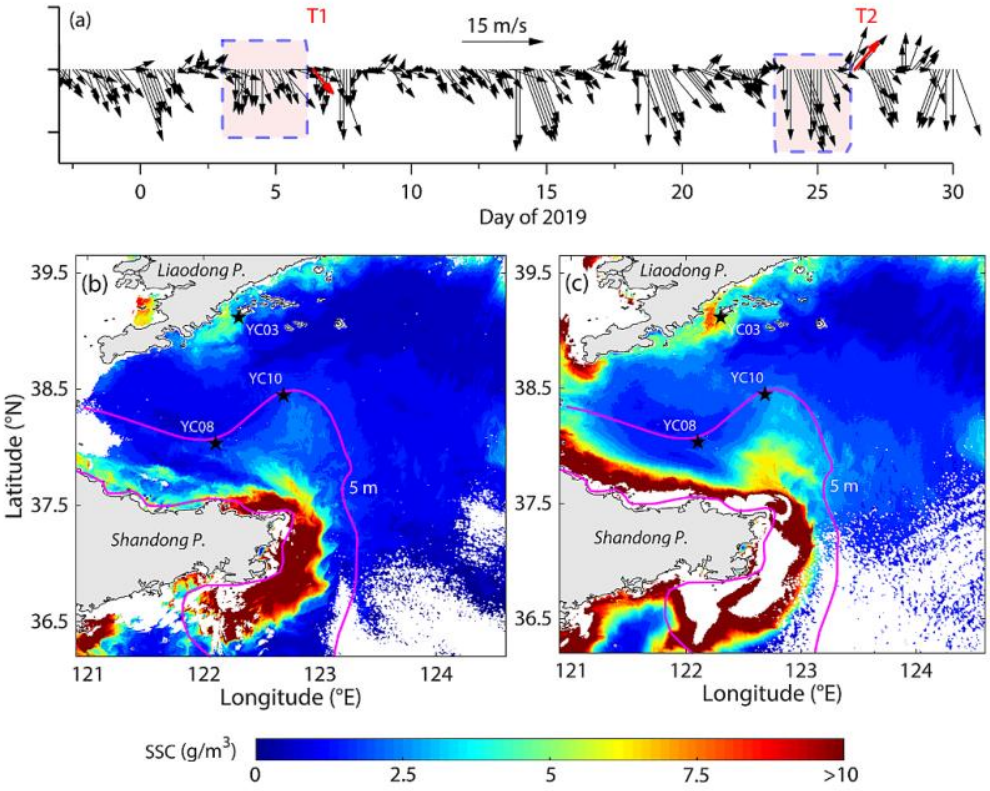

Figure 2. (a) Six-hour interval wind series during January 2019 for Chengshantou Station, located at the northeastern tip of the Shandong Peninsula. Two in-stances (T1 and T2) were captured by remote sensing imagery after winter storms (burst of northwesterly wind, shaded area in (a)). Cross-front sediment transport at T1(b) and T2 (c) were captured by remote sensing imagery. The shape of the 5 m isopach (pink line) indicates the strong relationship between the formation of the mud patch and cross-front sediment transport in the NYS.